2’-Fucosyllactose helps butyrate producers outgrow competitors in the infant gut

Versluis, D.; Schoemaker, R.; Looijesteijn, E.; Geurts, J.M.W.; Merks, R.M.H.

2'-Fucosyllactose helps butyrate producers outgrow competitors in infant gut microbiota simulations

David M. Versluis [1], Ruud Schoemaker [2], Ellen Looijesteijn [2], Jan M. W. Geurts [2], and Roeland M. H. Merks [*1,3]

[1]Leiden University, Institute of Biology, Leiden, The Netherlands

[2]FrieslandCampina, Amersfoort, the Netherlands

[3]Leiden University, Mathematical Institute, Leiden, The Netherlands

Abstract

A reduced capacity for butyrate production by the early infant gut microbiota is associated with negative health effects, such as inflammation and the development of allergies. Here we develop new hypotheses on the effect of the prebiotic galacto-oligosaccharides (GOS) or 2'-fucosyllactose (2'-FL) on butyrate production by the infant gut microbiota using a multiscale, spatiotemporal mathematical model of the infant gut. The model simulates a community of cross-feeding gut bacteria at metabolic detail. It represents the gut microbiome as a grid of bacterial populations that exchange intermediary metabolites, using 20 different subspecies-specific metabolic networks taken from the AGORA database. The simulations predict that both GOS and 2'-FL promote the growth of *Bifidobacterium*, whereas butyrate producing bacteria are only consistently abundant in the presence of propane-1,2-diol, a product of 2'-FL metabolism. The results suggest that in absence of prebiotics or in presence of only GOS, bacterial species, including *Cutibacterium acnes* and *Bacteroides vulgatus*, outcompete butyrate producers by feeding on intermediary metabolites. In presence of 2'-FL, however, production of propane-1,2-diol specifically supports butyrate producers.

Keywords: Infant microbiota, Microbial ecology, Flux balance analysis, Cellular automata, Cross-feeding, 2'-Fucosyllactose, Galacto-oligosaccharides

*r.m.h.merks@biology.leidenuniv.nl

1 Introduction

Infants develop a complex microbiota shortly after birth, which is important for healthy growth and development [70]. Here we focus on butyrate, a short-chain fatty acid (SCFA) that is produced in significant amounts by the gut bacteria [20] and is absorbed by the gut colonocytes. Production of butyrate by the microbiota has been suggested to improve the health of infants in a number of ways. Firstly, butyrate in the gut is a key energy source for the gut epithelium, making it important for maintaining the gut barrier function [58]. A breakdown of the gut barrier function due to a lack of butyrate is associated with diseases such as inflammatory bowel disease and rectal cancer [58, 82]. Butyrate production in young infants specifically is associated with a reduced risk of allergies and allergy-associated atopic eczema [11, 51, 81]. Infant butyrate producing bacteria provide protection against food allergies when transplanted into a mouse model [24], suggesting causality. Butyrate production is also associated with a reduced risk of colic in infants [17]. Butyrate also modulates the immune system throughout the body, inhibiting inflammation and carcinogenesis [33]. These data suggest it may be desirable to stimulate butyrate production in the infant gut. Using mechanistic computational modeling, here we investigate how stimulation of butyrate producing bacteria may be achieved in the early infant gut microbiota through supplementation with prebiotics.

Microbiota composition and metabolism are influenced by endogenous factors, e.g., gut maturity and inflammation, and exogenous factors, e.g., nutrition, probiotics, and antibiotics. Here we focus on nutrition, which is the primary exogenous factor. Human milk and many infant formulas contain prebiotics such as galacto-oligosaccharides (GOS) and 2'-fucosyllactose (2'-FL), which influence the composition of the gut microbiota and are associated with beneficial health effects for the infant, such as a decreased risk to require antibiotics [7] and reduced manifestation of allergies [49, 67, 28]. It has been hypothesized that some of the health effects associated with prebiotics may be linked to indirect stimulation of butyrate producing bacteria [73, 81]. Thus, both the capacity for butyrate production [11, 81], and prebiotics in nutrition by itself, particularly 2'-FL, have been linked to reduced manifestations of allergies [49, 67, 28].

Butyrate producing bacteria such as *Anaerobutyricum hallii* cannot directly consume GOS or 2'-FL, but they can consume metabolites of GOS or 2'-FL digestion [64]. The primary consumers of GOS and 2'-FL in the infant gut are *Bifidobacterium* spp.[8, 9]. Metabolites produced by *Bifidobacterium* spp., in turn, become important food sources for butyrate producing bacteria.

For example, *in vitro* it has been found that the butyrate producing bacterium *A. hallii* (formerly *Eubacterium hallii* [65]) can feed on lactate and propane-1,2-diol (1,2-PD), which are metabolites of *Bifidobacterium* spp. [64]. *A. hallii* can also coexist with *Bifidobacterium longum* ssp. *infantis* *in vitro* on a substrate of glucose or 2'-FL [64].

Despite these in vitro findings that demonstrate potential coexistence of *Bifidobacterium* spp. and butyrate producing bacteria, *in vivo*, i.e. in the infant gut microbiota, butyrate producing bacteria often only have a low abundance and butyrate is found in the feces of only 35% of infants [3]. It is unclear why butyrate producing bacteria and butyrate are not commonly abundant *in vivo*, given that *in vitro* cross-feeding on lactate occurs readily [64], and that lactate-producing *Bifidobacterium* species are abundant in the gut of most infants [4, 69]. Using computational modeling we explore the conditions that may stimulate butyrate producing bacteria *in vivo* in the infant gut. To this end we will compare simulations of simple microbial communities, such as those studied *in vitro*, with simulations of more complex communities that may more closely resemble the *in vivo* situation.

Briefly, the computational model suggests that in simple microbial communities, populations of butyrate producing bacteria can cross-feed on *Bifidobacterium* metabolites. However, in more complex communities the intermediary metabolites are consumed by competitors instead of butyrate producing bacteria. In the presence of 2'-FL, populations of butyrate producing bacteria are nevertheless supported. The mechanism suggested by our simulations is that *Bifidobacterium* produces 1,2-PD from 2'-FL, which specifically feeds butyrate producing species, allowing these to outgrow competing cross-feeders. We provide predictions for interactions in *in vivo* and *in vitro* systems and suggestions for *in vitro* verification of these predictions.

2 Results

2.1 Model outline

To develop new hypotheses on how oligosaccharides can stimulate the production of butyrate, we further develop a multiscale metabolic model (Fig. 1A & B) of the carbon metabolism of the infant gut microbiota [78]. The computational model is based upon our earlier models of the adult and infant microbiota [75, 78]. In comparison with these previous models, the present model simulates a larger number of small bacterial populations, using a larger, more

diverse, and further curated set of metabolic models of gut bacteria from the AGORA database [44]. In particular, we have included the butyrate producers *A. hallii*, *Roseburia inulinivorans* and *Clostridium butyricum* and the digestion of the prebiotic oligosaccharides GOS and 2'-FL by *Bifidobacterium longum* ssp. *infantis*. The complete community model integrates these predictions of metabolism over space and time to create a multiscale model that covers the development and variation of the infant gut microbiota over the first three weeks of life. Other multiscale metabolic modelling techniques have been used previously to model the adult human microbiota in frameworks such as SteadyCom and Comets [12, 21]. The model presented here distinguishes itself from these frameworks by its focus on the infant gut microbiota, by including factors such as prebiotics and the initial presence of oxygen at birth.

Briefly, the spatial model simulates the ecology of an intestinal microbial ecosystem, and features genome-scale metabolic models (GEMs) of intestinal bacteria, spatial structuring, exchange of extracellular metabolites, and population dynamics. The system is simulated on a regular square lattice of 225×8 boxes of 2×2 mm, representing a typical infant colon of 45×1.6 cm. Each box contains a simulated metapopulation of one of a set of up to 20 of the most common bacterial species present in the infant gut [4] (Table 1), and concentrations of simulated nutrients and metabolites such as extracellular oligosaccharides and short-chain fatty acids. Based on the concentrations of metabolites, the systems predicts the growth rate for each metapopulation as well as the uptake and excretion rates of metabolites using a GEM taken from AGORA [43], a database of metabolic networks of intestinal bacteria. The system is initialised by distributing, on average, 540 populations over the system at random. Oxygen is introduced during initialisation, and water is always available.

After initialisation, the model is simulated in timesteps representing three minutes of real time. Each timestep of the simulation proceeds as follows. Every 3 hours (i.e., 60 timesteps), a mixture of simulated lactose and/or oligosaccharides is added to the leftmost six columns of lattice sites. Then, each step, the model predicts the metabolism of each local population using flux balance analysis (FBA) based on the metabolites present in the local lattice site, the GEM of the species, and the enzymatic constraint. The enzymatic constraint limits the total amount of metabolism that can be performed by each local population per timestep by limiting the maximum summed flux for each FBA solution. The enzymatic constraint is determined by the local population size. This approach allows us to model metabolic switches and trade-offs

Table 1: Species and subspecies included in the model. Colour indicates colour used in figures.

Name	Phylum	Anaerobic status per [44]	Butyrate producing
Bifidobacterium longum ssp. *infantis*	Actinomycetota	Obligate anaerobe	no
Bifidobacterium longum ssp. *longum*	Actinomycetota	Obligate anaerobe	no
Collinsella aerofaciens	Actinomycetota	Obligate anaerobe	no
Cutibacterium acnes	Actinomycetota	Facultative anaerobe	no
Rothia mucilaginosa	Actinomycetota	Microaerophile	no
Eggerthella sp. *YY7918*	Actinomycetota	Nanaerobe	no
Streptococcus oralis	Bacillota	Facultative anaerobe	no
Staphylococcus epidermidis	Bacillota	Facultative anaerobe	no
Gemella morbillorum	Bacillota	Facultative anaerobe	no
Enterococcus faecalis	Bacillota	Facultative anaerobe	no
Lactobacillus gasseri	Bacillota	Facultative anaerobe	no
Ruminococcus gnavus	Bacillota	Obligate anaerobe	no
Veillonella dispar	Bacillota	Obligate anaerobe	no
Anaerobutyricum hallii	Bacillota	Obligate anaerobe	yes
Roseburia inulinivorans	Bacillota	Obligate anaerobe	yes
Clostridium butyricum	Bacillota	Obligate anaerobe	yes
Parabacteroides distasonis	Bacteroidota	Nanaerobe	no
Bacteroides vulgatus	Bacteroidota	Nanaerobe	no
Haemophilus parainfluenzae	Pseudomonadota	Aerobe	no
Escherichia coli SE11	Pseudomonadota	Facultative anaerobe	no

[45, 78]. The FBA solution includes a set of influx rates and efflux rates of metabolites that are used to update the environmental metabolite concentrations. The local populations are assumed to grow at a rate linearly proportional to the rate of ATP production[63], which is predicted by FBA by optimizing for ATP production rates. Populations may create a new population in a neighbouring lattice site if the local population is 200 times the initial size (Fig. 1A-1). Populations of more than 400 times the local size, which can only form when density if so high new populations cannot be created, stop metabolism to represent quiescence. Populations spread at random into adjacent lattice sites (Fig. 1A-2); metabolites diffuse and advect towards the back of the tube (Fig. 1A-3&4). To mimic excretion, metabolites and populations are deleted from the most distal column each timestep. To represent bacterial colonisation, new populations of randomly selected species are introduced into empty lattice sites at a small probability. All parameters are given in table 2. Details of the model are given in section Methods.

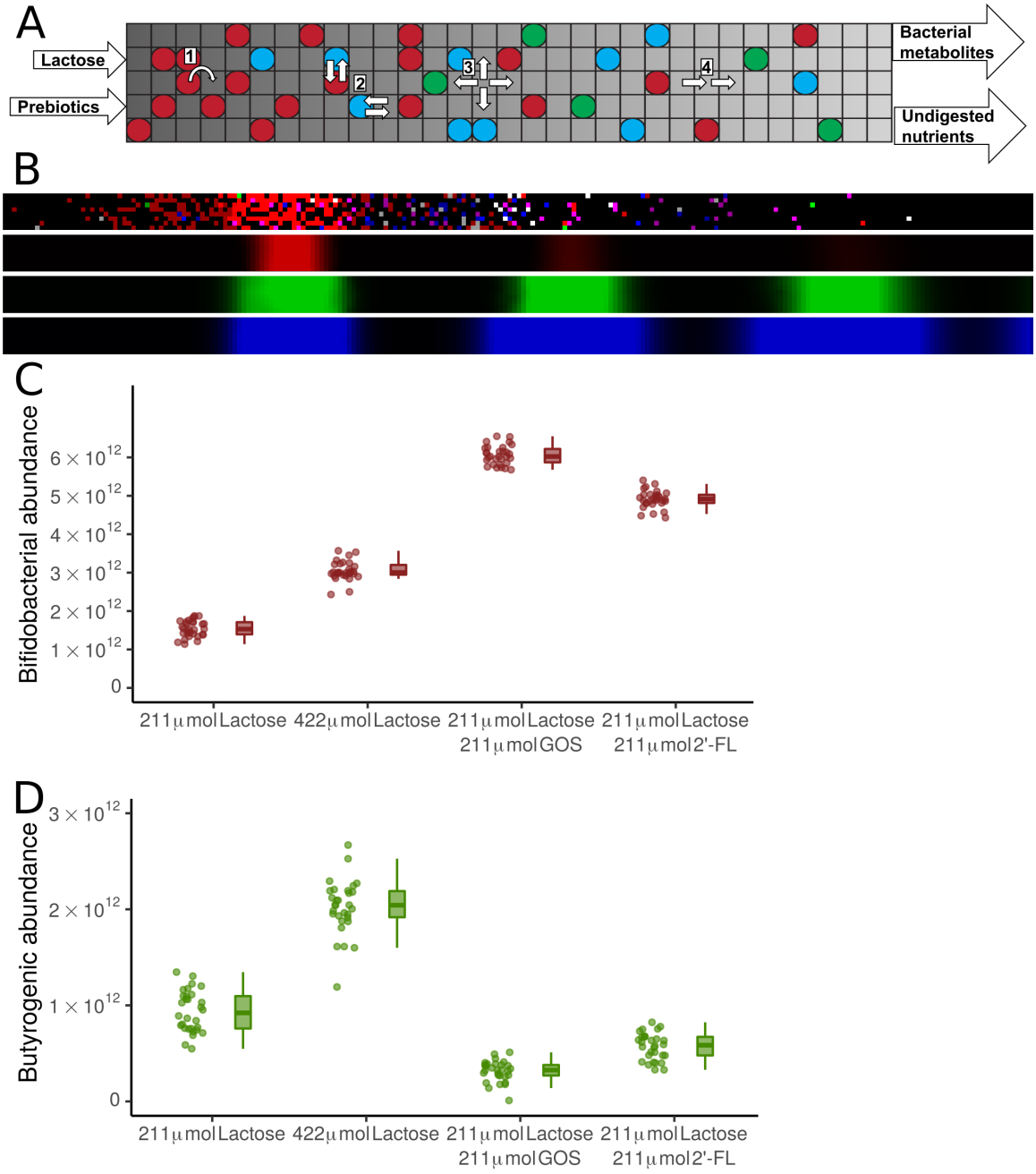

Figure 1: **Model predicts coexistence of *Bifidobacterium* and butyrate producing bacteria in absence of competition**
(A) Schematic of the model. Circles represent bacterial populations, colour represents species. Flow through the tube is from left (proximal) to right (distal). Nutrients entered the system proximally. All metabolites leave the system distally. Lattice dimensions are schematic.
(B) Screenshots of the model at a single time point, showing, from top to bottom, the bacterial layer, lactose, lactate, and acetate. Brightness indicates growth in the bacterial layer, and concentration in the metabolic layers.
(C,D) Abundance of (C) *Bifidobacterium* spp., (D) butyrate producing bacteria, at the end of 21 days for 30 sets of simulations with no prebiotics, no prebiotics and additional lactose, with GOS, or with 2'-FL at the end of 21 days. n=30 for each condition, each simulation is represented by one dot.

Table 2: Parameters of the model

Parameter	Value	Unit
Lattice side length	2	mm
Width of lattice	225	lattice sites
Height of lattice	8	lattice sites
Timestep	180	seconds
Average number of initial populations	540	-
New population placement probability	0.00005	per timestep per empty lattice site
Population death probability	0.0075	per timestep per population
Initial size per population	$5 \cdot 10^7$	no. of bacteria
Population size to create a new population	$1 \cdot 10^{10}$	no. of bacteria
Maximum population size	$2 \cdot 10^{10}$	no. of bacteria
ATP to grow one cell	$1 \cdot 10^{-15}$	mol
Enzymatic constraint	2	µmol flux per timestep per $1 \cdot 10^{10}$ bacteria
Nutrient input	211	µmol per nutrient per 60 timesteps
Initial oxygen	0.1	µmol per lattice site
Metabolic advection	2	mm per timestep
Diffusion (metabolites and bacteria)	$6.3 \cdot 10^5$	square cm per second

2.2 Model with simplified consortium of species predicts coexistence of butyrate producing bacteria and *Bifidobacterium*

We first simulated the model using a simplified consortium of species, the two *Bifidobacterium longum* subspecies (table 1) and three butyrate producing species: *Anaerobutyricum hallii*, *Clostridium butyricum*, and *Roseburia inulinivorans*. We performed 30 simulations for each of four conditions, in which the following sugars were introduced every three simulated hours: (1) 211 µmol lactose and no prebiotics, (2) 422 µmol lactose and no prebiotics, (3) 211 µmol lactose plus 211 µmol GOS, and (4) 211 µmol lactose plus 211 µmol 2'-FL. We estimated 211 µmol lactose to be a realistic amount of lactose to reach the infant colon, given infant intake and small intestinal uptake [5, 12]. As there is little absorption by the small intestine of prebiotics [27], the amount of prebiotics in the nutrition consumed by the infant would be much smaller than the amount of lactose. We also include the 422 µmol lactose condition to control for the possibility that effects in the conditions with prebiotics are due the larger amount of sugar present conditions, instead of their type. The condition with 422 µmol lactose does not correspond to an *in vivo* condition. We analyzed the abundance of each species at the end of 10080 timesteps, representing 21 simulated days. In each of the four conditions *Bifidobacterium* bacteria (Fig. 1C) and butyrate producing bacteria coexisted (Fig. 1D), and, paradoxically, butyrate producing bacteria were reduced in presence of prebiotics.

2.3 In presence of competitors, model predicts coexistence of butyrate producing bacteria and *Bifidobacterium* in the presence of 2'FL but not in presence of GOS

We next examined the behaviour of the system in the presence of a more complex consortium, consisting of all 20 species and subspecies listed in Table 1, simulating the same four conditions. In absence of prebiotics, regardless of the quantity of lactose, the model predicted that *Bifidobacterium*, *Bacteroides* and *Escherichia* became the most abundant genera after three weeks (Fig. 2A, S1 Video), consistent with *in vivo* observation [4, 69]. We also observed some abundance of Bacilli in accordance with *in vivo* observations [4, 19, 69]. The higher quantity of lactose resulted in a higher average abundance for all major groups. In absence of prebiotics, butyrate producing bacteria achieved a combined abundance over $1 \cdot 10^{10}$ in only 4 of the 30 simulations with 211 µmol of lactose per 3 hours, and 6 of the 30 with 422 µmol of lactose (Fig. 2B). In the remaining simulations, the butyrate producing bacteria remained almost absent, staying below $1 \cdot 10^{10}$ bacteria. In the simulations with GOS, *Bifidobacterium* was more abundant than in the condition without prebiotics ($p<0.001$,Fig. 2A) whereas the butyrate producing bacteria were not affected ($p=0.18$) (Fig. 2B). With GOS, butyrate producing bacteria also had a combined abundance of over $1 \cdot 10^{10}$ bacteria at the end of 13 of the 30 simulations (Fig. 2B). Interestingly, in the condition with 2'-FL the abundance of butyrate producing bacteria was over $1 \cdot 10^{10}$ bacteria at the end of 19 of 30 simulations (Fig. 2B), and the butyrate producing species were more abundant (Fig. 2A, S2 Video) than in the other conditions. Thus 2'-FL but not GOS stimulated butyrate producing bacteria in the complex community. To test for any concentration-dependence or cross-talk between 2'-FL and GOS we next performed sets of 30 simulations in presence of 211 µmol lactose and levels of 2'-FL and GOS varying between 21.1 µmol to 211 µmol per three hours and combinations thereof (Fig. S1). The amount of 2'-FL ($p=0.017$, Kruskal-Wallis rank sum test) but not that of GOS ($p=0.658$, Kruskal-Wallis rank sum test) affected the abundance of butyrate producing bacteria, further supporting the prediction that 2'-FL but not GOS stimulates butyrate producing bacteria in the complex community.

In order to investigate why 2'-FL led to a more consistent abundance of butyrate producing bacteria we analysed the metabolic interactions between bacterial species. We visualised the network of metabolic fluxes between the bacteria using arrows between species and metabolite

pools in Fig. 2C-E. The resulting diagrams show both primary consumption, i.e., uptake of nutrients such as lactose, GOS, and 2'-FL, and cross-feeding, i.e., uptake of metabolites produced by other species. Sample visualisations of the condition without prebiotics (211 µmol lactose) (Fig. 2C, S3 Video) and the condition with GOS (Fig. 2D) revealed co-occurrence of species and cross-feeding, but no butyrate production. In these simulations the cross-feeding metabolite lactate, which is a known substrate for butyrate producing bacteria [64], was consumed by *Bacteroides vulgatus* and *Cutibacterium acnes*, respectively. Butyrate formation only occurred in the sample simulation with 2'-FL (Fig. 2E). Only in presence of 2'-FL and not in the other conditions, was a flux of 1,2-PD directed towards the butyrate producing species (Fig. 2E and S4 Video). We therefore hypothesised that butyrate producing species may be more abundant in the model simulations with 2'-FL, because 2'-FL digestion by *Bifidobacterium* produces 1,2-PD as a cross-feeding substrate. 1,2-PD is a known *Bifidobacterium* metabolite from 2'-FL *in vitro* [64]. To test this hypothesis, we performed new sets of simulations with 2'-FL in which we blocked the uptake by butyrate producing bacteria of either lactose, lactate, or 1,2-PD, i.e, the uptake of metabolites most consumed by butyrate producing bacteria was disabled. Indeed, blocking the uptake of any of these metabolites led to a reduction of butyrate producing bacteria (Fig. 2F). Thus a flux of lactose, lactate, but also 1,2-PD that is only produced in presence of 2'-FL, was required for sustaining butyrate producing bacteria in our simulations.

We next turned to the model with the simplified consortium of species, the two *Bifidobacterium* subspecies and three butyrate producing species, to test if uptake of lactose, lactate and 1,2-PD was also required for butyrate producing bacteria to become abundant with this consortium. After blocking the uptake of lactose, lactate, or 1,2-PD by butyrate producing bacteria, the abundance of butyrate producing bacteria was reduced at the end of the simulations compared to the control (Fig. 3A). Surprisingly, however, and in contrast to the complete system (Fig. 2F), butyrate producing populations retained an abundance over $1 \cdot 10^{10}$ bacteria in respectively 27 and 30 of 30 simulations when lactose or 1,2-PD uptake was disabled. Thus neither lactose nor 1,2-PD were essential for butyrate producing bacteria. Altogether, 1,2-PD, and thus 2'-FL, was required for butyrate producing bacteria in the complex system, but not in the simplified system. Thus these model simulations suggest that supplementation with 2'-FL introduces a flux of 1,2-PD from *Bifidobacterium* spp. to butyrate producing bacteria that prevents competitive exclusion of butyrate producers by competitors such as *B. vulgatus* (fig. 2C) or *C. acnes* (fig. 2D).

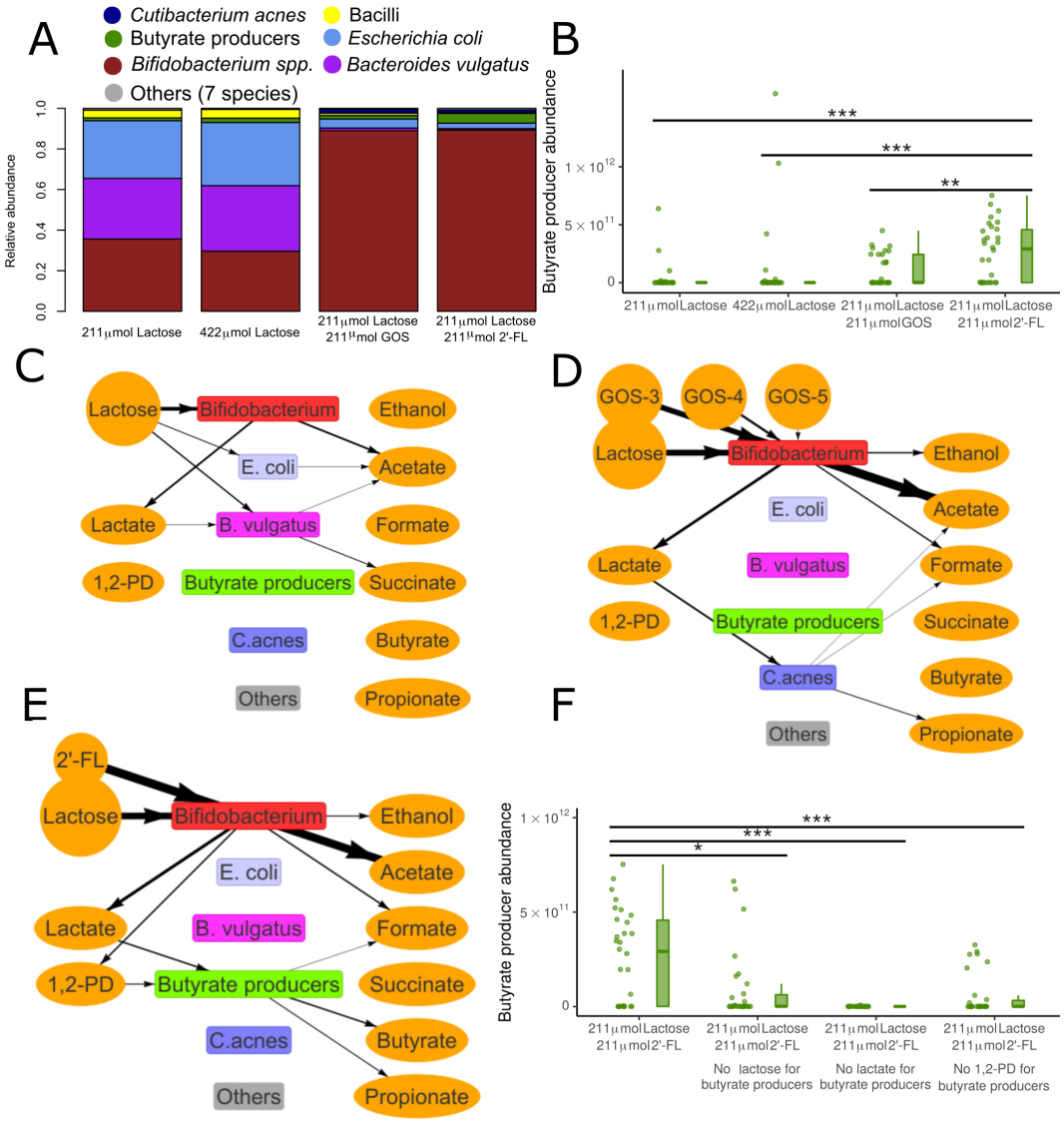

Figure 2: **Unlike GOS, 2'-FL leads to stimulation of butyrate producing bacteria through 1,2-PD in the full simulated microbiota**

(A) Relative abundance of bacterial species in the condition with no prebiotics, no prebiotics and additional lactose, with GOS, or with 2'-FL at the end of 21 days. n=30 for each condition, each simulation is weighed equally. The key to the species in each group is in table 1.

(B) Abundance of butyrate producing bacteria at the end of 21 days for the four conditions of A. n=30 for each condition. Each simulation is represented by one dot. $p<0.001$ for 2'-FL compared to no prebiotics and no prebiotics with additional lactose. $p=0.004$ for 2'-FL compared to GOS.

(C,D,E) Visualisation of metabolic interactions in a sample simulation (C) without prebiotics (211 µmol lactose per three hours) (D) with GOS (DP3,DP4, and DP5 displayed separately) (E) with 2'-FL. Line width is scaled with the flux per metabolite over the last 60 timesteps, multiplied by the carbon content of the molecule, with a minimum threshold of 100 µmol atomic carbon. Data from last 3 hours, step 10020 to 10080. Circles indicate nutrients.

(F) Abundance of butyrate producing bacteria with 2'FL at the end of 21 days. Uptake of lactose, lactate, or 1,2-PD by butyrate producing bacteria is disabled in the 'no lactose', 'no lactate', and 'no 1,2-PD' conditions respectively. $p=0.010$,$p<0.001$,$p<0.001$ for each disabled uptake compared to the baseline, respectively n=30 for each condition. Each simulation is represented by one dot.

NS: Not significant, *: $p<0.05$, **:$p<0.01$, ***:$p<0.001$

2.4 *Bacteroides vulgatus* and *C. acnes* are effective competitors on different substrates

In the 2'-FL condition butyrate producing bacteria fed on lactate and 1,2-PD (Fig. 2E). In the conditions without 2'-FL no 1,2-PD was produced and lactate was consumed by *B. vulgatus* or *C. acnes* (Fig. 2C&D). This suggests that, in absence of 1,2-PD, *B. vulgatus* and *C. acnes* outcompete the butyrate producing bacteria for lactate. To investigate whether these species could indeed be responsible for outcompeting butyrate producing bacteria we again turned to the model with the simplified consortium and added the potential competitors *B. vulgatus* and *C. acnes* to the consortium one by one.

First we studied the simplified consortium in absence of prebiotics in the conditions with 211 µmol and 422 µmol lactose per three hours. The abundance of butyrate producing bacteria was reduced in presence of *B. vulgatus* but not in presence of *C. acnes* (Fig. 3B, 422 µmol visualized in Fig. S3). After blocking lactose or lactate uptake by *B. vulgatus* in the condition with 211 µmol lactose, the abundance of butyrate producing bacteria was restored (Fig. 3B), indicating that *B. vulgatus* required both lactose and lactate to effectively outcompete the butyrate producing bacteria.

In the conditions with GOS, the situation was reversed: *C. acnes* but not *B. vulgatus* outcompeted butyrate producing bacteria (Fig. 3C). After blocking uptake of lactate by *C. acnes* the abundance of butyrate producing bacteria was restored (Fig. 3C). *C. acnes* does not use lactose in the model. Taken together, these simulations suggest that lactate is required for competitive exclusion of butyrate producing bacteria by *C. acnes*.

In the condition with 2'-FL *B. vulgatus* did not outcompete butyrate producing bacteria (Fig. 3D). *C. acnes* ($p=0.001$) moderately suppressed butyrate producing bacteria, with 29 of 30 simulations still predicting an abundance of butyrate producing bacteria of over $1 \cdot 10^{10}$ bacteria. This agrees with the simulations using the full consortium (Fig. 2B), which also displayed a robust abundance of butyrate producing bacteria in the 2'-FL condition.

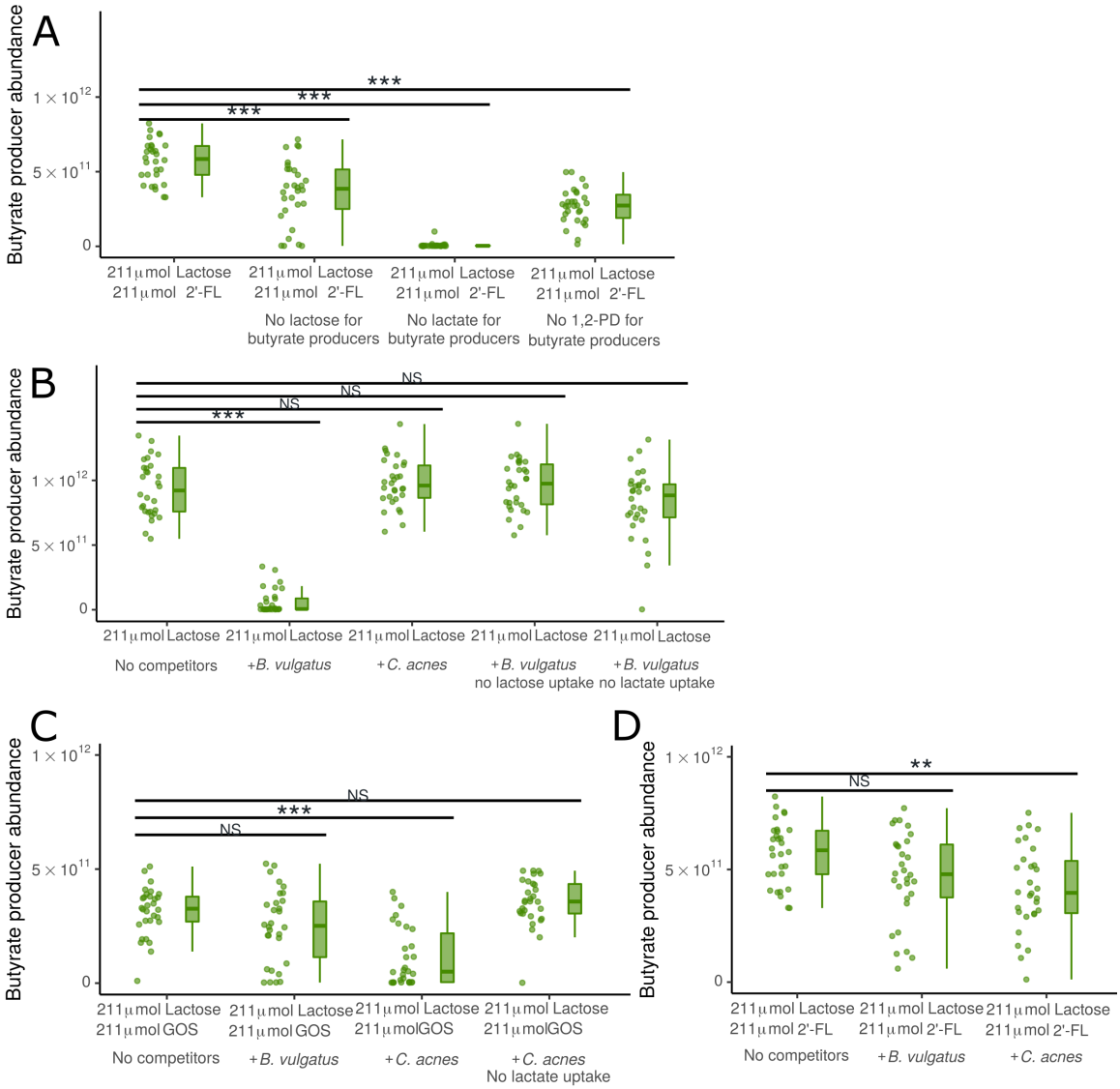

Figure 3: **2'-FL makes butyrate producing bacteria resistant to competition by other infant gut bacteria**

(A) Abundance of butyrate producers with 2'-FL and without competitors (only *Bifidobacterium* and butyrate producers) at the end of 21 days. Uptake of lactose, lactate, or 1,2-PD is disabled for butyrate producers in the 'no lactose', 'no lactate', and 'no 1,2-PD' conditions respectively. n=30 for each condition. Each simulation is represented by one dot. ($p<0.001$ for each disabled uptake compared to the baseline)

(B,C,D) Abundance of butyrate producers at the end of 21 days (B) without prebiotics, either without competitors (only *Bifidobacterium* and butyrate producers), with addition of *B. vulgatus*, with addition of *B. vulgatus* unable to take up either lactose or lactate, or with addition of *C. acnes*. n=30 for each condition. Each simulation is represented by one dot. $p<0.001$ for abundance of butyrate producers with *B. vulgatus* compared to no competitors

(C) with GOS, either without competitors (only *Bifidobacterium* and butyrate producers), with addition of *C. acnes*, with addition of *C. acnes* unable to take up lactate, or with addition of *B. vulgatus*. n=30 for each condition. Each simulation is represented by one dot. $p<0.001$ for abundance of butyrate producers with *C. acnes* compared to no competitors

(D) with 2'-FL, either without competitors (only *Bifidobacterium* and butyrate producers), with addition of *C. acnes*, or with addition of *B. vulgatus*. n=30 for each condition. Each simulation is represented by one dot. $p=0.001$ for abundance of butyrate producers with *C. acnes* compared to no competitors. NS: Not significant, *: $p<0.05$, **:$p<0.01$, ***:$p<0.001$

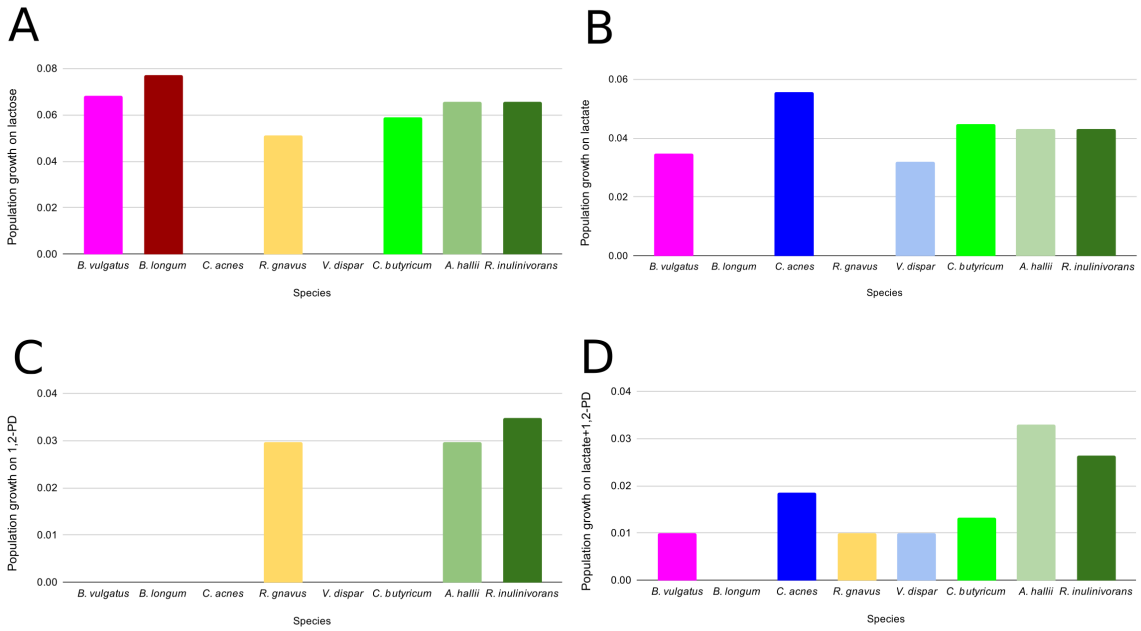

Figure 4: **Populations of butyrate producing bacteria only grow much faster than their competitors on a mixed substrate of 1,2-PD and lactate**
(A) Growth on unlimited lactose and water over a single timestep for butyrate producing bacteria (three rightmost bars, in green) compared to other lactose-fermenting bacteria in the model.
(B) Growth on unlimited lactate and water over a single timestep for butyrate producing bacteria (three rightmost bars, in green) compared to other lactate-fermenting bacteria in the model.
(C) Growth on unlimited 1,2-PD, acetate, and water over a single timestep for butyrate producing bacteria (two rightmost bars, in green) compared to another 1,2-PD-fermenting bacterial species in the model.
(D) Growth on 1 µmol per ml of 1,2-PD and lactate, and unlimited acetate and water, over a single timestep for butyrate producing bacteria (three rightmost bars, in green) compared to other bacteria in the model for populations of $5 \cdot 10^9$ bacteria with access to one lattice site (0.05ml)

2.5 Butyrate producing bacteria can use a mixture of lactate and 1,2-PD as substrates in the 2'-FL condition to grow faster than their competitors

To analyse how butyrate producing bacteria can outcompete other species only in the presence of 2'-FL but not in the presence of GOS or without prebiotics, we next examined the growth rates per timestep on unlimited quantities of the three key substrates for butyrate producing bacteria indicated above: lactose, lactate, and 1,2-PD. With unlimited availability of lactose, the growth of the three butyrate producing species was reduced relative to the growth of most other species (Fig. 4A). With unlimited lactate, growth for butyrate producing species was superior to the other species, but not to *C. acnes* (Fig. 4B). In presence of unlimited 1,2-PD and acetate the butyrate producing species *A. hallii* and *Roseburia inulinivorans* grew faster than the other species (Fig. 4C). On a mixture of limited lactate and 1,2-PD, with acetate available, two of the three butyrate producing species also grew faster compared to all other species (Fig. 4D). Thus the unique ability of butyrate producing bacteria to grow on 1,2-PD and acetate in the model allowed them to outcompete other lactate-consuming species in environments with 1,2-PD, such as those where *Bifidobacterium* consumes 2'-FL. However, they would be unable to outcompete the same species in conditions without 1,2-PD.

2.6 Sensitivity analysis

Finally, to test the generality of our observations we performed a sensitivity analysis on the system. The enzymatic constraint (Fig. S2A&B), the death rate and growth rate (through the ATP required per population unit) (Fig. S2C&D), the placement of new populations of random species in empty lattice sites (colonization) (Fig. S2E&F), the diffusion of metabolites and populations (Fig. S2G&H),the amount of initial oxygen (Fig. S2I&J), and quiescence for large populations (Fig. S2K) were varied. We used three conditions for most changed parameters: 211 µmol lactose, 211 µmol lactose plus 211 µmol GOS, and 211 µmol lactose plus 211 µmol 2'-FL per three hours. We only used the latter two for disabling quiescence, as no populations entered quiescence during our initial runs with 211 µmol lactose. We found minor sensitivity for most parameter changes (Fig. S2). We found the most notable effects when we disabled colonization or initial oxygen. When we disabled colonization the abundance of butyrate producing bacteria was lower in all three conditions ($p<0.001$ for all). The absence of

initial oxygen increased the abundance of butyrate producing bacteria in the condition without prebiotics and with 2'-FL (p=0.002,p=0.035). This indicates that the presence of initial oxygen and sustained colonization are particularly important in the simulated system.

3 Discussion

This paper describes a computational study of the effects of the prebiotics GOS and 2'-FL on butyrate producing bacteria in the infant gut microbiota. We have used the model to generate novel hypotheses to explain the — sometimes counter-intuitive — mechanisms at the biochemical and population level that underlie the effects of prebiotics. The model predicts that butyrate producing bacteria can coexist with *Bifidobacterium* in the infant gut with or without GOS or 2'-FL as long as no other bacterial species are present. As soon as other bacterial species are introduced into the model, we found that they can act as competitors, thus reducing the abundance of butyrate producing bacteria. Specifically, the model predicts that *B. vulgatus* outcompetes butyrate producing bacteria in absence of prebiotics. The predicted mechanism is that *B. vulgatus* consumes lactose and lactate, important food sources of the butyrate producing species. In presence of GOS, the model predicts that *C. acnes* becomes the key competitor of the butyrate producing bacteria due to its lactate consumption. In presence of 2'-FL, however, the butyrate producing species are no longer outcompeted. The mechanism as predicted by the model is as follows. The breakdown of 2'-FL by *Bifidobacterium* produces 1,2-PD. 1,2-PD becomes an additional food source for the butyrate producing bacteria, helping them to outgrow competitors. Thus, our modeling results predict that only 2'-FL, but not GOS supports populations of butyrate producing bacteria in their competition against species such as *B. vulgatus* and *C. acnes*.

The following *in vitro* and *in vivo* observations agree with these model predictions. Firstly, the model predicts co-existence and crossfeeding between *Bifidobacterium* and butyrate producing species on 2'-FL. In agreement with the model predictions, co-existence of and cross-feeding between *Bifidobacterium* and butyrate producing bacteria occurs *in vitro* within simplified, synthetic communities on glucose, fucose, and 2'-FL in the absence of competitors [64]. Secondly, the model predicts that in presence of the competitors such as *B. vulgatus* and *C. acnes*, *B. vulgatus* will become abundant in absence of prebiotics and outcompete butyrate producing species. In agreement with this model prediction, *B. vulgatus* is often abundant in the *in vivo*

infant gut microbiota [4], and it can consume lactose *in vitro* [66]. No information is available on lactate consumption of *B. vulgatus*, but the related *Bacteroides fragilis* is able to consume lactate *in vitro* [42]. Thirdly, the model predicts that *C. acnes* outcompetes butyrate producing bacteria in presence of GOS by consuming lactate. In agreement with this prediction, *C. acnes* is found in 22% of infants [4] and *Cutibacterium avidum*, closely related to *C. acnes* [62], reduces the abundance of the butyrate producer *A. hallii* in an *in vitro* lactate-fed microbiota from infant fecal samples [56]. Both *C. acnes* and *C. avidum* consume lactate *in vitro* [29]. Finally, the model predicts that butyrate producing bacteria become competitive through cross-feeding on 1,2-PD, which is produced by *Bifidobacterium longum* from 2'-FL. In agreement with this prediction, the butyrate producer *A. hallii* cross-feeds on 1,2-PD in an *in vitro* synthetic community of *A. hallii* and *B. longum* [64]. Also in line with this prediction, 2'-FL supplementation increased the abundance of butyrate producing bacteria in *in vitro* fecal communities based on infant fecal samples, which likely include key competitors of butyrate producing species [73]. An *in vitro* colonic fermentation model inoculated with infant feces has previously been used to study the effect of introducing specific competitors to a lactate-consuming infant gut microbiota [56]. This approach could also be used to test if *B. vulgatus* and *C. acnes* are viable competitors in the infant gut and if the presence of 1,2-PD allows butyrate producing species to outcompete other bacteria.

More broadly, the model simulations without prebiotics predict that *Escherichia*, *Bacteroides*, and *Bifidobacterium* become the three most abundant genera, which agrees with the most abundant genera found in the infant gut microbiota around the age of three weeks [4, 69]. The relative abundances the model predicts for butyrate producing species range from 1.4% without prebiotics to 4.8% with 2'-FL, both of which are within the broad range of values reported for the butyrate producing community [3]. However, for two less abundant groups, Bacilli and *Veillonella*, the model predictions disagree with *in vivo* data. Firstly, an initially dominant Bacilli phase is sometimes seen *in vivo*, e.g. in 17.6% of subjects in [19], but not in any model outcomes. An initially dominant Bacilli phase is associated in non-premature infants with a shorter gestational period [19], but it is unclear exactly what factors are responsible. A similar initial dominance of Bacilli that often occurs in premature infants has been hypothesised to be related to selection pressures by the immune system, a different composition of initial colonizers [39], or a defective mucin barrier [18]. Secondly, the model predicted a very low *Veillonella dispar* abundance in all conditions. These predictions contradict *in vivo* data [55, 4] in which

V. dispar is relatively abundant. *V. dispar* likely has a lower abundance in the model due to an incorrectly reduced growth rate relative to the other species in the model on lactate, the primary energy source of *V. dispar* [60], lactate, (Fig. 4B). We do not expect a large influence on the overall model predictions from this discrepancy, as *C. acnes* has a metabolism similar to that of *V. dispar* in the model and *in vitro*: both produce propionate, consume lactate, and cannot consume lactose [29]. However, we cannot exclude that other species in the model, such as *Veillonella* spp., may be more important competitors *in vivo* than the competitors that the model predicts.

Potential sources of the discrepancies between model predictions and experimental data include: (1) errors in the metabolic predictions of the underlying FBA models; (2) computational errors, and (3) incomplete representation of the biology underlying infant digestion. A typical error occurring in FBA models is an incomplete prediction of metabolic shifts, which is in part due to the assumption of FBA models that the growth rate or energy production is optimised [52]. For example, the FBA model does not correctly predict the metabolic shift from high-yield to low-yield metabolism as observed *in vitro* in *Bifidobacterium* growing on increasing concentrations of GOS and 2'-FL [84, 16]. FBA only predicts high-yield metabolism. The model, therefore, likely underestimates total lactate production. The effects of this discrepancy on the results are difficult to predict, but as lactate is a cross-feeding substrate, the underestimation of lactate may cause the model to underestimate the abundance of cross-feeding species such as *C. acnes* or butyrate producing bacteria. The optimality assumption of FBA also ignores any other 'task' that a bacterium has, besides growth. For example, sporulation, toxin production, or metabolic anticipation [48] may limit biomass production. The model does not represent such genetically regulated mechanisms.

Further errors in the model predictions can be due to simplifications in the FBA model. For example, we assume that the total flux through the reaction networks is capped (Eq. 4), so as to mimic the maximum volume in a cell that can be filled with enzymes. Here each enzyme is assumed to have equal maximum flux, and the optimization problem then predicts the optimal relative flux distribution. In reality, due to differences in enzyme concentration and enzyme efficiency these maximum fluxes can of course differ, which affects the predictions of FBA [6, 74]. If species-specific data on efficiency and genetic regulation of pathways become available, such weighting could be included in the model. The metabolic predictions from the FBA

layer could be further improved in future versions of the model by integrating thermodynamic plausibility and favorability into FBA, which have previously improved metabolic predictions for intracellular metabolism [34, 25]. Additionally, the FBA model includes an extracellular compartment in which long GOS chains are broken down to shorter GOS chains, but it is not possible for extracellular breakdown products to diffuse during this process. Such extracellular digestion may lead to additional competition effects, because competitors may 'steal' digestion products without investing in the enzymes themselves [30]. Such effects may become important if additional species are introduced in the model that digest prebiotics extracellularly, such as *Bifidobacterium bifidum* [8].

Computational errors in the model (2) include the discretization of time, the discretization of space, and rounding errors in the FBA solver. Firstly, all processes in the model are assumed to be constant within each timestep, which means the model only roughly approximates the continuous temporal dynamics of processes such as metabolism and diffusion. Secondly, we discretize the three-dimensional continuous cylindrical space of the gut into a two-dimensional rectangular grid of lattice sites. We consider each lattice site to be of equal volume and to have equal flow through it. This simplification introduces many errors, as lattice sites must represent different shapes of three-dimensional space, and these shapes are not connected as they would be in three-dimensional space. It is difficult to estimate what impact these discretizations have on the model. Finally, the FBA solver uses floating point arithmetic to generate a deterministic but not exact solution to each FBA problem. These distortions are very small, typically on the order of 10^{-15} µmol per metabolite per FBA solution, so we do not expect a notable effect on the results.

Errors in the model predictions due to an incomplete representation of the biology underlying infant digestion (3) include missing organisms, missing ecological interactions, the simplifications we made to the metabolic input, and missing representation of host interactions. Firstly, the model does not include fungi or archaea in the infant gut. Both groups occur at a lower absolute abundance than the bacterial microbiota, but may still influence it [59]. Secondly, the model does not include interactions between bacteria other than cross-feeding and competition for resources. Missing interactions include acidification of the gut [14], the production of bacteriocins [22] and the effects of phage infections [47], all of which have species-specific effects. Thirdly, the model does not include the input of fats, proteins, or minerals into the gut. This

means that the model cannot represent stimulation of growth by digestion of fats or proteins, nor potential limits on growth due to, for example, the lack of iron [46] or essential amino acids [41]. Finally, the model does not represent the interactions of the host with the microbiota, such as the continuous secretion by the gut wall of mucin [37] and oxygen [1], and the uptake of short-chain fatty acids [79]. Colonic mucins in particular could greatly influence the microbiota, as *B. bifidum* consumes colonic mucins extracellularly, which facilitates cross-feeding by butyrate producing bacteria *in vitro* [10].

Despite the inevitable limitations of the model, we have shown here how the model can be used to produce testable predictions on the effects of prebiotics and competition on butyrate producing bacteria in the infant gut microbiota. Future versions of the model may be a useful help in follow-up studies on the effects of nutrition on bacterial population dynamics in the infant and adult gut microbiota.

4 Methods

We used a spatially explicit model to represent the newborn infant gut microbiota. The model is based on our earlier models of a general microbiota [75] and the infant microbiota [78]. Prebiotic digestion is the most important addition in the present version of the model.

The model consists of a regular square lattice of 225×8 lattice sites, with each lattice site representing 2×2 mm of space. Taken together this represents an infant colon of 450×16 mm, in line with *in vivo* estimates [72, 15]. Each lattice site can contain an amount of the 735 metabolites represented in the model, as well as a single bacterial population.

4.1 Species Composition

Species were selected based on [4], using sheet 2 of their Table S3. We selected the 20 entries with the highest prevalence in vaginally delivered newborns. After removing two duplicate entries we selected a representative species for each genus from the AGORA database [43]. We then added an additional *Bifidobacterium longum* ssp. *infantis* GEM to serve as prebiotic consumer, and a *Roseburia inulinivorans* GEM. *Roseburia* spp. have been shown to be a prevalent butyrate producing bacterium in infants in other studies [3]. Together, these form the list of species (Table 1).

4.2 Changes from AGORA

The model uses GEMs generated in the AGORA project [44]. We have applied various changes and additions to these models (Table S1).

We have added digestion of GOS or 2'-FL to the *B. longum* ssp. *infantis* GEM as follows. 2'-FL digestion was implemented by adding reactions representing an ABC-transporter and an intracellular fucosidase that breaks 2'-FL down to lactose and fucose [84]. GOS was represented through separate DP3, DP4, and DP5 fractions [77]. The DP4 and DP5 fractions are broken down extracellularly to DP3 and DP4 fractions respectively, releasing one galactose molecule in the process [76]. The DP3 fraction is taken up with an ABC transporter, and broken down internally to lactose and galactose [76].

We have also further expanded earlier curation of the AGORA GEMs [78]. We disabled anaerobic L-lactate uptake for the *Bifidobacterium* GEMs and for *E. coli* in line with available literature [23, 13]. To have the GEMs correspond with existing literature on lactose uptake we added a lactose symporter to *Anaerobutyricum hallii* [10], both *Bifidobacterium longum* GEMs [54], *Roseburia inulinivorans* [57], *Haemophilus parainfluenzae* [32], and *Rothia mucilaginosa* [71]. We also added galactose metabolism to *R. inulinivorans* [35] and *R. mucilaginosa* [71]. Further changes were made to prevent unrealistic growths and the destruction of atoms within reactions (Table S1).

4.3 Validity checks

After applying the changes in Table S1 we tested all GEMs individually for growth on a substrate of lactose and water. In line with literature, this did not lead to growth for *Veillonella disparans* [60], *Cutibacterium acnes* [29], *Eggerthella* sp. YY7918 [83], and *Gemella morbillorum* [80]. All other species grew on this substrate. We also checked for any spurious growth by checking each GEM for growth with only water present.

During each simulation, the model checks the FBA solutions for thermodynamic plausibility. The model uses a database of Gibbs free energy values [50] for all metabolites except 2'-FL and GOS. Values for 2'-FL and GOS were generated from the values for lactose and fucose, and lactose and galactose, respectively. Separate values were generated for the separate fractions of GOS. All values assumed a pH of 7 and an ionic strength of 0.1 M. We found that in the simulations of Fig. 2A with the baseline level of lactose, combined with those with GOS and

2'-FL (n=90) 99.98% of all FBA solutions had a lower or equal amount of Gibbs free energy in the output compared to the input. The remaining 0.02% of FBA solutions was responsible for 0.003% of total bacterial growth.

4.4 FBA with enzymatic constraint

Although other aspects of the model were changed, the FBA approach we used is identical to that used in the earlier model [78]. The model uses a modified version of flux balance analysis with an enzymatic constraint to calculate the metabolic inputs and outputs of each population at each timestep [52, 45]. Each GEM is first converted to a stoichiometric matrix S. Reversible reactions are converted to two irreversible reactions, so that flux is always greater than or equal to 0. Reactions identified in the GEM as 'exchange', 'sink', or 'demand' in the GEM are also recorded as 'exchange' reactions. These exchange reactions are allowed to take up or deposit metabolites into the environment. Each timestep, all reactions are assumed to be in internal steady state:

$$S \cdot \vec{f} = 0, \tag{1}$$

where $\vec{f}$ is a vector of the metabolic fluxes through each reaction in the network, in mol per time unit per population unit.

Each exchange reaction that takes up metabolites from the environment F_{in} is constrained by an upper bound F_{ub} which represents the availability of metabolites from the environment. It is determined as follows:

$$\vec{F_{in}} \leq \vec{F_{ub}}, \tag{2}$$

where $\vec{F_{in}}$ is a vector of fluxes between the environment and the bacterial population. $\vec{F_{ub}}$ is a vector of upper bounds on these fluxes. $\vec{F_{ub}}$ is set dynamically at each timestep t by the spatial environment at each lattice site $\vec{x}$:

$$\vec{F_{ub}}(\vec{x}, t) = \frac{\vec{c}(\vec{x}, t)}{B(\vec{x}, t)}, \tag{3}$$

where $\vec{c}$ is a vector of all metabolite concentrations in mol per lattice site, $\vec{x}$ is the location and $B(\vec{x},t)$ is the size of the local bacterial population. The size of B can range from $5\cdot10^7$ to $2\cdot10^{10}$ bacterial cells.

Finally the enzymatic constraint constrains the total flux through the network. It represents the maximum, total amount of flux that can be performed per cell in each population:

$$\sum \vec{f} \leq a. \tag{4}$$

The enzymatic constraint a is in mol per time unit per population unit. As both $\vec{f}$ and a are per population unit, this limit scales with population size, so each bacterial cell contributes equally to the metabolic flux possible in a lattice site. The enzymatic constraint is included as a constraint on each FBA solution. Given the constraints, FBA identifies the solution that optimises the objective function, ATP production. The solution consists of a set of input and output exchange fluxes $\vec{F_{in}}(\vec{x},t)$ and $\vec{F_{out}}(\vec{x},t)$, and a growth rate $g(\vec{x},t)$. The exchange fluxes are taken as the derivatives of a set of partial-differential equations to model the exchange of metabolites with the environment. The size of the population increases proportionally to the growth rate in the FBA solution.

To mimic quiescence at high densities, populations above the spreading threshold of $2\cdot10^{10}$ bacteria do not perform metabolism. In practice this rarely occurs because we maintain sufficient space for populations to spread into empty lattice sites. In the simulations of Fig. 2A (n=120) metabolism was not performed in, on average, 0.05% of all populations in a timestep.

4.5 Environmental metabolites

We model 735 different extracellular metabolites. This is the union of all metabolites that can be exchanged with the environment by at least one GEM in the model. In the simulations 39 metabolites are present in the medium in more than micromolar amounts at any point. We combine the L-lactate and D-lactate metabolites for fig. 1B, Video S1 and Video S2. Nearly all lactate in the model is L-lactate.

To represent the mixing of metabolites by colonic contractions we apply a diffusion process to the metabolites at each timestep. Metabolic diffusion is applied in two equal steps to the model. In each step, 14.25% of each metabolite diffuses from each lattice site to each of the four nearest

neighbours. This causes a net diffusion each timestep of $6.3 \cdot 10^5$ cm^2/s. Metabolites are also added and removed by bacterial populations as a result of the FBA solutions, yielding

$$\frac{d\vec{c}(\vec{x},t)}{dt} = \vec{F_{out}}(\vec{x},t)B(\vec{x},t) - \vec{F_{in}}(\vec{x},t)B(\vec{x},t) + \frac{D}{L^2}\sum_{\vec{i}\in \mathrm{NB}(\vec{x})}\left(\vec{c}(\vec{i},t) - \vec{c}(\vec{x},t)\right), \tag{5}$$

where $\vec{F_{out}}(\vec{x},t)$ is a vector of fluxes from the bacterial populations to the environment, in mol per time unit per population unit, D is the diffusion constant, L is the lattice side length, and $NB(\vec{x})$ are the four nearest neighbours.

All metabolites except oxygen are moved distally by one lattice site every timestep to represent advection. The transit time, including diffusion, is approximately 11 hours, corresponding with *in vivo* observations in newborn infants [61, 36]. Metabolites at the most distal column of the lattice, the end of the colon, are removed from the system at each timestep.

Every 60 timesteps (representing three hours) metabolites representing inflow from the small intestine are inserted into the first six columns of lattice sites. Three hours represents a realistic feeding interval for neonates [31]. Food intake contains 211 µmol of lactose by default, a concentration in line with human milk [5], assuming 98% host uptake of carbohydrates before reaching the colon [12]. In some simulations 211 µmol of additional lactose, GOS, or 2'-FL is added. Because there is very little uptake of prebiotics by the infant [27], the oral intake of prebiotics would be much lower than that of lactose. GOS is inserted as separate fractions of DP3, DP4, or DP5 based on analysis of the composition of Vivinal-GOS [77]. 64% is DP3, 28% is DP4 and 8% is DP5. Water is provided in unlimited quantities. Oxygen is placed during initialisation [68] at 0.1 µmol per lattice site. No other metabolites are available, other than those produced as a result of bacterial metabolism within the model.

4.6 Population dynamics

During initialization there is a probability of 0.3 for each lattice site to get a population of size $5 \cdot 10^7$ of a random species (Table 1). Taken together, this averages around 540 populations, leading to a total initial bacterial load of $2.7 \cdot 10^{10}$, in line with *in vivo* estimates [53] when we assume a uniform bacterial density and a total colon volume of 90 ml. In each timestep each local population solves the FBA problem based on its own GEM, the enzymatic constraint a, its current population size $B(\vec{x},t)$ and the local concentrations of metabolites $\vec{c}(\vec{x},t)$, and applies

the outcome to the environment (see above) and the growth rate $g(\vec{x},t)$ to its own population size, as follows:

$$\frac{dB(\vec{x},t)}{dt} = B(\vec{x},t)g(\vec{x},t). \tag{6}$$

Each step, each population of at least $1 \cdot 10^{10}$ bacteria (Table 2) will create a new population if an adjacent empty lattice site is available. Half of the old population size is transferred to the new population, so that the total size is preserved. To mimic colonisation new populations are introduced at random into empty lattice sites during the simulation, representing both dormant bacteria from colonic crypts [40] and small bacterial populations formed from ingested bacteria, which may only become active after being moved far into the gut. Each empty lattice site has a probability of 0.00005 (Table 2) each step to acquire a new population of a randomly selected species. All species have an equal probability to be selected. We initialise these populations at the same population size B as the initial populations in the model (Table 2). Each population dies out at a probability of 0.0075 per timestep, creating a turnover within the range of estimated microbial turnover rates in the mouse microbiota [26].

To mix the bacterial populations the lattice sites swap population contents each timestep. We use an algorithm inspired by Kawasaki dynamics [38], also used previously for bacterial mixing [78, 75]: In random order, the bacterial content of each site, i.e., the bacterial population represented by its size $B(\vec{x},t)$ and the GEM, are swapped with a site randomly selected from the Moore neighbourhood. This swap only occurs if both the origin and destination site have not already swapped in this timestep. With this mixing method the diffusion constant of the bacterial populations is $6.3 \cdot 10^5 cm^2/s$, equal to that of the metabolites. Bacterial populations at the most distal column, i.e. at the exit of the colon, are removed from the system. To increase the bacterial diffusion rate in the sensitivity analysis this process was executed five times, marking all sites as unswapped after each execution. To decrease the bacterial diffusion rate the number of swaps was limited to a fifth of the usual number of swaps.

4.7 Analysis

We record the size, species, location, and important exchange fluxes $\vec{F_{in}}(\vec{x},t)$ and $\vec{F_{out}}(\vec{x},t)$ for each population at each timestep. To detect irregularities we also record the net flux of carbon,

hydrogen, oxygen, and Gibbs free energy for every population at each timestep. Gibbs free energy is estimated using the Equillibrator database [50]. Energy loss l in joules per timestep per population unit is recorded as follows, where i are metabolites, F is the exchange flux rate in mol per timestep per population unit and E contains the Gibbs free energy in joules per mol for each metabolite,

$$l = \sum_i F(i) \cdot E(i). \tag{7}$$

4.8 Parameters

Parameters of the system are listed in table 2. We estimate a total volume of 90ml for the infant colon [72, 15], which leads to a rough estimate on the order of 10^{12} bacteria in the newborn infant colon given an abundance per ml of around 10^{10} [53]. Values for free parameters were estimated and evaluated in the sensitivity analysis.

4.9 Implementation

We implemented the model in C++11. We based the model on our own earlier models of the gut microbiota [75, 78]. Random numbers are generated with Knuth's subtractive random number generator algorithm. Diffusion of metabolites was implemented using the Forward Euler method. The GEMs are loaded using libSBML 5.18.0 for C++. We used the GNU Linear Programming Kit 4.65 (GLPK) as a linear programming tool to solve each FBA with enzymatic constraint. We used the May 2019 update of AGORA, the latest at time of writing, from the Virtual Metabolic Human Project website (vmh.life). We used Python 3.6 to extract thermodynamic data from the eQuilibrator API (December 2018 update) [50]. When not noted otherwise p-values were calculated with R 4.2.1 using the Mann-Whitney test from the 'stats' package 3.6.2. Model screenshots were made using the libpng16 and pngwriter libraries. Other visualisations were performed with R 4.2.1 and Google Sheets. Raincloud visualisations used a modified version of the Raincloud plots library for R [2].

5 Supplemental material

S1 Table.

Table of changed or deleted reactions and annotations.csv

A table of changes made to the AGORA models as a .csv file.

S1 Video.

Video of a simulation with no prebiotics, consisting of a visualisation of the distribution of bacterial species and major metabolites. Lines represent, from top to bottom: Bacteria, lactose, 2'-FL, lactate (Both L and D), acetate, 1,2-PD, butyrate, succinate, CO2, H2, propionate

S2 Video.

Video of a simulation with 2'-FL, consisting of a visualisation of the distribution of bacterial species and major metabolites. Lines represent, from top to bottom: Bacteria, lactose, 2'-FL, lactate (Both L and D), acetate, 1,2-PD, butyrate, succinate, CO2, H2, propionate

S3 Video.

Video of a simulation without prebiotics, displaying fluxes between population and metabolite pools Line width is scaled with the flux per metabolite over 60 timesteps per frame, multiplied by the carbon content of the molecule, with a minimum threshold of 100 µmol atomic carbon.

S4 Video.

Video of a simulation with 2'-FL, displaying fluxes between population and metabolite pools. Line width is scaled with the flux per metabolite over the 60 timesteps per frame, multiplied by the carbon content of the molecule, with a minimum threshold of 100 µmol atomic carbon.

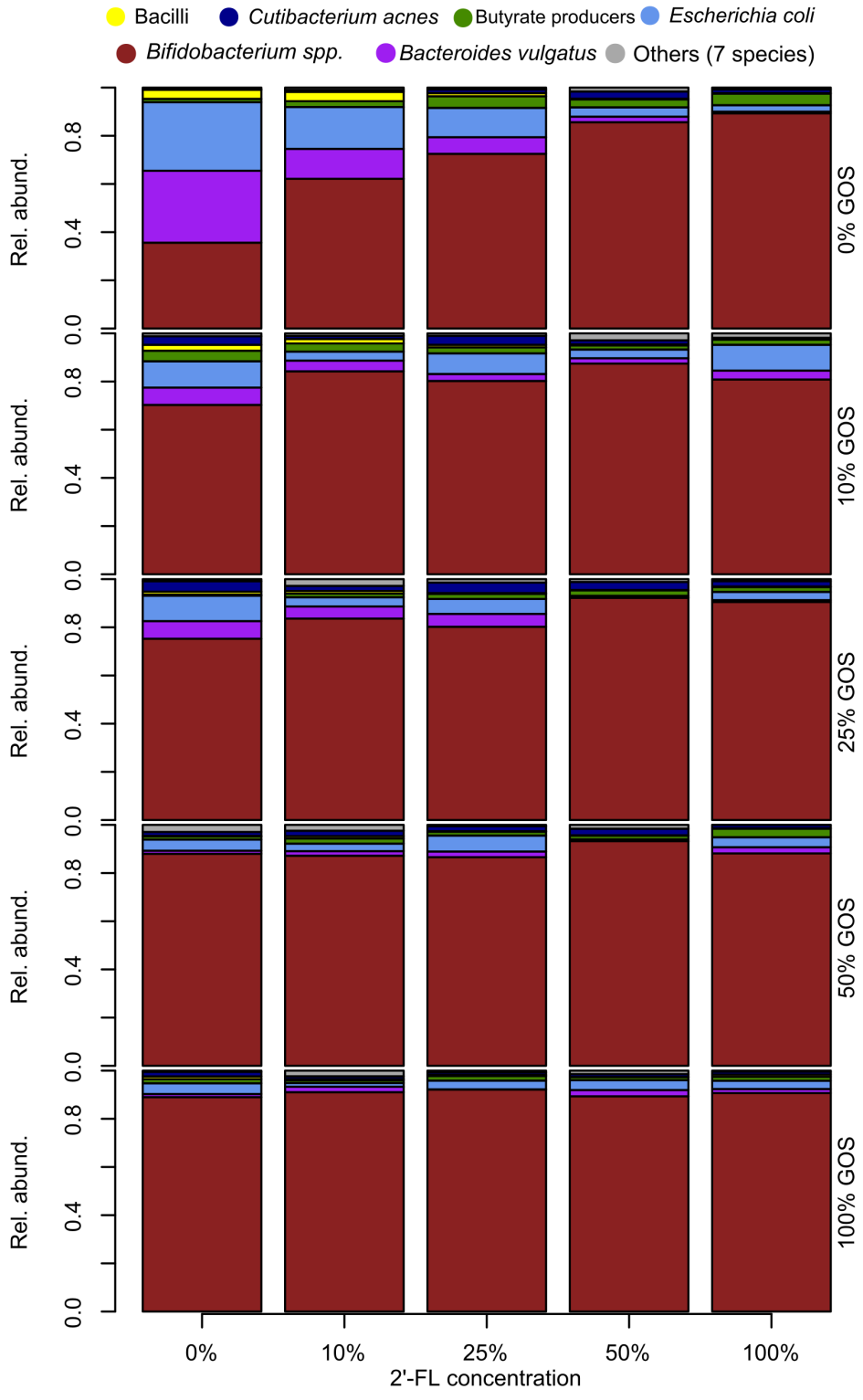

S1 Figure.

Relative abundance of bacterial species at the end of 21 days with varying inputs of 2'-FL and GOS compared to the fixed input amount of lactose. n=30 for each condition, each simulation is weighed equally.

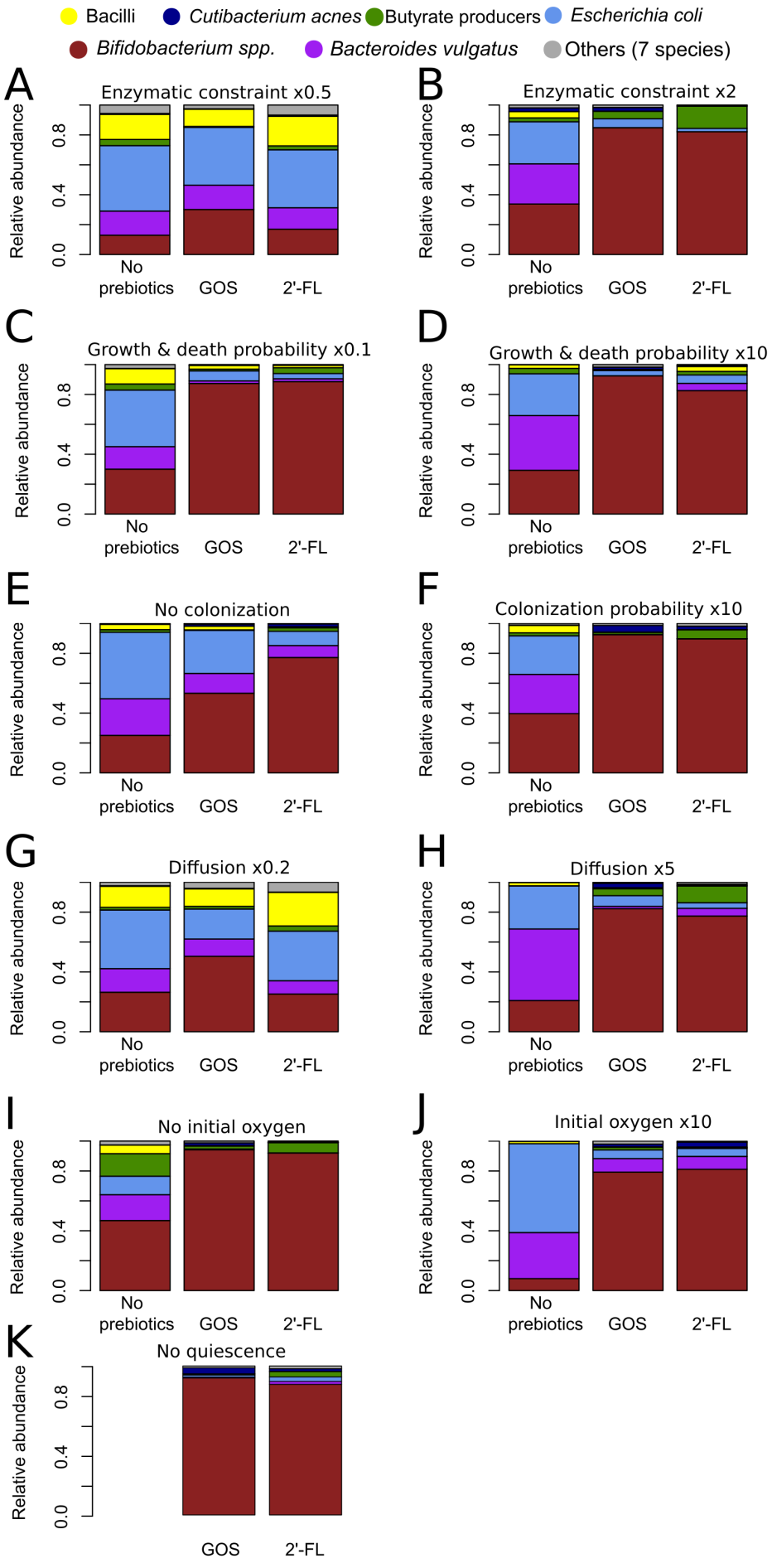

S2 Figure.

(A to K) Relative abundance of bacterial species in the conditions with no prebiotics, with GOS, or with 2'-FL at the end of 21 days, with the following alteration from the baseline of Fig. 2A: (A) Enzymatic constraint loosened by a factor of 2, to 4 µmol flux per timestep per $1 \cdot 10^{10}$ population (B) Enzymatic constrained tightened by a factor of 2, to 1 µmol flux per timestep per $1 \cdot 10^{10}$ population (C) Growth decreased by a factor of 10, by increasing the ATP per bacteria to $1 \cdot 10^{-14}$, with the death probability decreased to 0.00075 per population per timestep. (D) Growth increased by a factor of 10 by decreasing the ATP per bacteria to $1 \cdot 10^{-16}$, with the death probability increased to 0.075 per population per timestep (E) Colonisation removed by setting the probability for new populations to be placed after initialization to 0 (F) Colonisation increased by x10 by setting the probability per empty lattice to acquire a new population to 0.0005 per timestep (G) Diffusion of both metabolites and bacteria decreased by a factor of 5 to $1.26 \cdot 10^{-6}$ cm^2/s (H) Diffusion of both metabolites and bacteria increased by a factor of 5 to $3.15 \cdot 10^{-5}$ cm^2/s (I) No initial presence of oxygen (J) Initial oxygen increased to 1 µmol per lattice site (K) Quiescence disabled

For each figure: n=30 for each condition, each simulation is weighed equally.

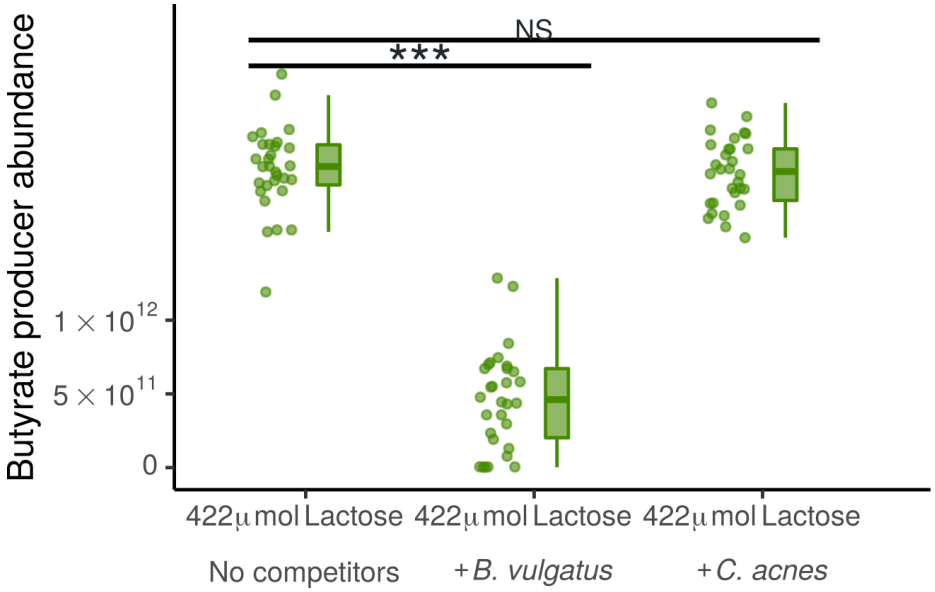

S3 Figure.

Abundance of butyrate producing bacteria at the end of 21 days with 422 µmol of lactose per three hours and without prebiotics, either without competitors (only *Bifidobacterium* and butyrate producing bacteria), with addition of *B. vulgatus*, or with addition of *C. acnes*. n=30 for each condition. Each simulation is represented by one dot.

NS: Not significant, *: p<0.05, **:p<0.01, ***:p<0.001

6 Contributions

J.M.W.G., and R.M.H.M acquired funding. D.M.V., J.M.W.G., and R.M.H.M. conceived and planned the simulations. D.M.V. wrote software used for the simulations. D.M.V. performed the simulations and analyzed the data. R.S, E.L., J.M.W.G., and R.M.H.M contributed to the interpretation of the results. J.M.W.G., and R.M.H.M. supervised the project. D.M.V. drafted the manuscript. D.M.V., R.S., E.L., J.M.W.G. and R.M.H.M. revised and edited the manuscript.

7 Acknowledgments

This study was financially supported by FrieslandCampina. R.S, E.L., and J.M.W.G. are currently employed by FrieslandCampina. This work was performed using the ALICE compute resources provided by Leiden University.

References

[1] Lindsey Albenberg, Tatiana V. Esipova, Colleen P. Judge, Kyle Bittinger, Jun Chen, Alice Laughlin, Stephanie Grunberg, Robert N. Baldassano, James D. Lewis, Hongzhe Li, Stephen R. Thom, Frederic D. Bushman, Sergei A. Vinogradov, and Gary D. Wu. Correlation between intraluminal oxygen gradient and radial partitioning of intestinal microbiota. *Gastroenterology*, 147(5):1055–1063.e8, 2014.

[2] Micah Allen, Davide Poggiali, Kirstie Whitaker, Tom Rhys Marshall, and Rogier A. Kievit. Raincloud plots: A multi-platform tool for robust data visualization [version 1; peer review: 2 approved]. *Wellcome Open Research*, 4:1–52, 2019.

[3] Olivia Appert, Alejandro Ramirez Garcia, Remo Frei, Caroline Roduit, Florentin Constancias, Vera Neuzil-Bunesova, Ruth Ferstl, Jianbo Zhang, Cezmi Akdis, Roger Lauener, Christophe Lacroix, and Clarissa Schwab. Initial butyrate producers during infant gut microbiota development are endospore formers. *Environmental Microbiology*, 22(9):3909–3921, 2020.

[4] Fredrik Bäckhed, Josefine Roswall, Yangqing Peng, Qiang Feng, Huijue Jia, Petia Kovatcheva-Datchary, Yin Li, Yan Xia, Hailiang Xie, Huanzi Zhong, Muhammad Tan-

weer Khan, Jianfeng Zhang, Junhua Li, Liang Xiao, Jumana Al-Aama, Dongya Zhang, Ying Shiuan Lee, Dorota Kotowska, Camilla Colding, Valentina Tremaroli, Ye Yin, Stefan Bergman, Xun Xu, Lise Madsen, Karsten Kristiansen, Jovanna Dahlgren, and Wang Jun. Dynamics and stabilization of the human gut microbiome during the first year of life. *Cell Host and Microbe*, 17(5):690–703, 2015.

[5] Olivia Ballard and Ardythe L. Morrow. Human Milk Composition. Nutrients and Bioactive Factors. *Pediatric Clinics of North America*, 60(1):49–74, 2013.

[6] Q. K. Beg, A. Vazquez, J. Ernst, M. A. De Menezes, Z. Bar-Joseph, A. L. Barabási, and Z. N. Oltvai. Intracellular crowding defines the mode and sequence of substrate uptake by Escherichia coli and constrains its metabolic activity. *Proceedings of the National Academy of Sciences of the United States of America*, 104(31):12663–12668, 2007.

[7] Bernard Berger, Nadine Porta, Francis Foata, Dominik Grathwohl, Michèle Delley, Deborah Moine, Aline Charpagne, Léa Siegwald, Patrick Descombes, Philippe Alliet, Giuseppe Puccio, Philippe Steenhout, Annick Mercenier, and Norbert Sprenger. Linking human milk oligosaccharides, infant fecal community types, and later risk to require antibiotics. *mBio*, 11(2):1–18, 2020.

[8] Markus Böger, Sander S. Van Leeuwen, Alicia Lammerts Van Bueren, and L. Dijkhuizen. Structural Identity of Galactooligosaccharide Molecules Selectively Utilized by Single Cultures of Probiotic Bacterial Strains. *Journal of Agricultural and Food Chemistry*, 67(50):13969–13977, 2019.

[9] Vera Bunesova, Christophe Lacroix, and Clarissa Schwab. Fucosyllactose and L-fucose utilization of infant Bifidobacterium longum and Bifidobacterium kashiwanohense. *BMC Microbiology*, 16(1):1–12, 2016.

[10] Vera Bunesova, Christophe Lacroix, and Clarissa Schwab. Mucin Cross-Feeding of Infant Bifidobacteria and Eubacterium hallii. *Microbial Ecology*, 75(1):228–238, 2018.

[11] Alissa Cait, Erick Cardenas, Pedro A. Dimitriu, Nelly Amenyogbe, Darlene Dai, Jessica Cait, Hind Sbihi, Leah Stiemsma, Padmaja Subbarao, Piush J. Mandhane, Allen B. Becker, Theo J. Moraes, Malcolm R. Sears, Diana L. Lefebvre, Meghan B. Azad, Tobias Kollmann, Stuart E. Turvey, and William W. Mohn. Reduced genetic potential for butyrate fermenta-

683 tion in the gut microbiome of infants who develop allergic sensitization. *Journal of Allergy*
684 *and Clinical Immunology*, 144(6):1638–1647.e3, 2019.

685 [12] Siu Hung Joshua Chan, Margaret N. Simons, and Costas D. Maranas. SteadyCom: Pre-
686 dicting microbial abundances while ensuring community stability. *PLoS Computational*
687 *Biology*, 13(5):1–25, 2017.

688 [13] David P. Clark. The fermentation pathways of Escherichia coli. *FEMS Microbiology Letters*,
689 63(3):223–234, 1989.

690 [14] Jonas Cremer, Markus Arnoldini, and Terence Hwa. Effect of water flow and chemical
691 environment on microbiota growth and composition in the human colon. *Proceedings of*
692 *the National Academy of Sciences of the United States of America*, 114(25):6438–6443,
693 2017.

694 [15] William S. Davis, R. Parker Allen, Blaise E. Favara, and Thomas L. Slovis. Neonatal small
695 left colon syndrome. *American journal of Roentgenology*, 120(2):322–329, 1974.

696 [16] L. De Vuyst, F. Moens, M. Selak, A. Rivière, and F. Leroy. Summer Meeting 2013: Growth
697 and physiology of bifidobacteria. *Journal of Applied Microbiology*, 116(3):477–491, 2014.

698 [17] Carolina De Weerth, Susana Fuentes, Philippe Puylaert, and Willem M. De Vos. Intestinal
699 microbiota of infants with colic: Development and specific signatures. *Pediatrics*, 131(2),
700 2013.

701 [18] Shaillay Dogra, Olga Sakwinska, Shu E. Soh, Catherine Ngom-Bru, Wolfram M. Brück,
702 Bernard Berger, Harald Brüssow, Neerja Karnani, Yung Seng Lee, Fabian Yap, Yap Seng
703 Chong, Keith M. Godfrey, and Joanna D. Holbrook. Rate of establishing the gut microbiota
704 in infancy has consequences for future health. *Gut Microbes*, 6(5):321–325, 2015.

705 [19] Shaillay Dogra, Olga Sakwinska, Shu-E. E. Soh, Catherine Ngom-Bru, Wolfram M. Brück,
706 Bernard Berger, Harald Brüssow, Yung Seng Lee, Fabian Yap, Yap-Seng Seng Chong,
707 Keith M. Godfrey, Joanna D. Holbrook, and GUSTO Study Group. Dynamics of infant
708 gut microbiota are influenced by delivery mode and gestational duration and are associated
709 with subsequent adiposity. *mBio*, 6(1):1–9, 2015.

710 [20] Dallas R. Donohoe, Nikhil Garge, Xinxin Zhang, Wei Sun, Thomas M. O'Connell, Mau-
711 reen K. Bunger, and Scott J. Bultman. The microbiome and butyrate regulate energy

metabolism and autophagy in the mammalian colon. *Cell Metabolism*, 13(5):517–526, 2011.

[21] Ilija Dukovski, Djordje Bajić, Jeremy M. Chacón, Michael Quintin, Jean C.C. Vila, Snorre Sulheim, Alan R. Pacheco, David B. Bernstein, William J. Riehl, Kirill S. Korolev, Alvaro Sanchez, William R. Harcombe, and Daniel Segrè. A metabolic modeling platform for the computation of microbial ecosystems in time and space (COMETS). *Nature Protocols*, 2021.

[22] G. A. Dykes and J. W. Hastings. Selection and fitness in bacteriocin-producing bacteria. *Proceedings of the Royal Society B: Biological Sciences*, 264(1382):683–687, 1997.

[23] Gwen Falony, Katerina Lazidou, An Verschaeren, Stefan Weckx, Dominique Maes, and Luc De Vuyst. In vitro kinetic analysis of fermentation of prebiotic inulin-type fructans by Bifidobacterium species reveals four different phenotypes. *Applied and Environmental Microbiology*, 75(2):454–461, 2009.

[24] Taylor Feehley, Catherine H. Plunkett, Riyue Bao, Sung Min Choi Hong, Elliot Culleen, Pedro Belda-Ferre, Evelyn Campbell, Rosita Aitoro, Rita Nocerino, Lorella Paparo, Jorge Andrade, Dionysios A. Antonopoulos, Roberto Berni Canani, and Cathryn R. Nagler. Healthy infants harbor intestinal bacteria that protect against food allergy. *Nature Medicine*, 25(3):448–453, 2019.

[25] R. M.T. Fleming, I. Thiele, and H. P. Nasheuer. Quantitative assignment of reaction directionality in constraint-based models of metabolism: Application to Escherichia coli. *Biophysical Chemistry*, 145(2-3):47–56, 2009.

[26] R. J. Gibbons and B. Kapsimalis. Estimates of the overall rate of growth of the intestinal microflora of hamsters, guinea pigs, and mice. *Journal of Bacteriology*, 93(1):510–512, 1967.

[27] Mark J. Gnoth, Clemens Kunz, Evamaria Kinne-Saffran, and Silvia Rudloff. Human milk oligosaccharides are minimally digested in vitro. *Journal of Nutrition*, 130(12):3014–3020, 2000.

[28] Karen C. Goehring, Barbara J. Marriage, Jeffery S. Oliver, Julie A. Wilder, Edward G. Barrett, and Rachael H. Buck. Similar to those who are breastfed, infants fed a formula

containing 2'-fucosyllactose have lower inflammatory cytokines in a randomized controlled trial. *Journal of Nutrition*, 146(12):2559–2566, 2016.

[29] Michael Goodfellow, Peter Kämpfer, Hans-Jürgen Busse, Martha E Trujillo, Ken-ichiro Suzuki, Wolfgang Ludwig, and William B Whitman. *Bergey's Manual® of Systematic Bacteriology: Volume Five The Actinobacteria, Part A*. Springer, 2012.

[30] Jeff Gore, Hyun Youk, and Alexander Van Oudenaarden. Snowdrift game dynamics and facultative cheating in yeast. *Nature*, 459(7244):253–256, 2009.

[31] Laurence M. Grummer-Strawn, Kelley S. Scanlon, and Sara B. Fein. Infant feeding and feeding transitions during the first year of life. *Pediatrics*, 122(SUPPL. 2), 2008.

[32] Kamal A. Hamed, Philip R. Dormitzer, Catherine K. Su, and David A. Relman. Haemophilus parainfluenzae endocarditis: application of a molecular approach for identification of pathogenic bacterial species. *Clinical Infectious Diseases*, 19(4):677–683, 1994.

[33] H. M. Hamer, D. Jonkers, K. Venema, S. Vanhoutvin, F. J. Troost, and R. J. Brummer. Review article: The role of butyrate on colonic function. *Alimentary Pharmacology and Therapeutics*, 27(2):104–119, 2008.

[34] Laurent Heirendt, Sylvain Arreckx, Thomas Pfau, Sebastián N. Mendoza, Anne Richelle, Almut Heinken, Hulda S. Haraldsdóttir, Jacek Wachowiak, Sarah M. Keating, Vanja Vlasov, Stefania Magnusdóttir, Chiam Yu Ng, German Preciat, Alise Žagare, Siu H. J. Chan, Maike K. Aurich, Catherine M. Clancy, Jennifer Modamio, John T. Sauls, Alberto Noronha, Aarash Bordbar, Benjamin Cousins, Diana C. El Assal, Luis V. Valcarcel, Iñigo Apaolaza, Susan Ghaderi, Masoud Ahookhosh, Marouen Ben Guebila, Andrejs Kostromins, Nicolas Sompairac, Hoai M. Le, Ding Ma, Yuekai Sun, Lin Wang, James T. Yurkovich, Miguel A. P. Oliveira, Phan T. Vuong, Lemmer P. El Assal, Inna Kuperstein, Andrei Zinovyev, H. Scott Hinton, William A. Bryant, Francisco J. Aragón Artacho, Francisco J. Planes, Egils Stalidzans, Alejandro Maass, Santosh Vempala, Michael Hucka, Michael A. Saunders, Costas D. Maranas, Nathan E. Lewis, Thomas Sauter, Bernhard Ø. Palsson, Ines Thiele, and Ronan M. T. Fleming. Creation and analysis of biochemical constraint-based models using the COBRA Toolbox v.3.0. *Nature Protocols*, 14(3):639–702, mar 2019.

[35] Ethan T. Hillman, Ariangela J. Kozik, Casey A. Hooker, John L. Burnett, Yoojung Heo, Violet A. Kiesel, Clayton J. Nevins, Jordan M.K.I. Oshiro, Melissa M. Robins, Riya D.

771 Thakkar, Sophie Tongyu Wu, and Stephen R. Lindemann. Comparative genomics of the
772 genus Roseburia reveals divergent biosynthetic pathways that may influence colonic com-
773 petition among species. *Microbial Genomics*, 6(7):7–24, 2020.

774 [36] Jeffrey S. Hyams, M. Alex Geertsma, Nancy L. Etienne, and William R. Treem. Colonic
775 hydrogen production in infants with colic. *The Journal of Pediatrics*, 115(4):592–594, 1989.

776 [37] Sercan Karav, Giorgio Casaburi, and Steven A. Frese. Reduced colonic mucin degradation
777 in breastfed infants colonized by Bifidobacterium longum subsp. infantis EVC001. *FEBS*
778 *Open Bio*, 8(10):1649–1657, 2018.

779 [38] Kyozi Kawasaki. Diffusion constants near the critical point for time-dependent ising models.
780 I. *Physical Review*, 145(1):224–230, 1966.

781 [39] Patricio S. La Rosa, Barbara B. Warner, Yanjiao Zhou, George M. Weinstock, Erica Soder-
782 gren, Carla M. Hall-Moore, Harold J. Stevens, William E. Bennett, Nurmohammad Shaikh,
783 Laura A. Linneman, Julie A. Hoffmann, Aaron Hamvas, Elena Deych, Berkley A. Shands,
784 William D. Shannon, and Phillip I. Tarr. Patterned progression of bacterial populations in
785 the premature infant gut. *Proceedings of the National Academy of Sciences of the United*
786 *States of America*, 111(34):12522–12527, 2014.

787 [40] S. Melanie Lee, Gregory P. Donaldson, Zbigniew Mikulski, Silva Boyajian, Klaus Ley, and
788 Sarkis K. Mazmanian. Bacterial colonization factors control specificity and stability of the
789 gut microbiota. *Nature*, 501(7467):426–429, 2013.

790 [41] Petra Louis and Harry J. Flint. Formation of propionate and butyrate by the human colonic
791 microbiota. *Environmental Microbiology*, 19(1):29–41, 2017.

792 [42] J. M. Macy, L. G. Ljungdahl, and G. Gottschalk. Pathway of succinate and propionate
793 formation in Bacteroides fragilis. *Journal of Bacteriology*, 134(1):84–91, 1978.

794 [43] Stefanía Magnúsdóttir, Almut Heinken, Laura Kutt, Dmitry A. Ravcheev, Eugen Bauer,
795 Alberto Noronha, Kacy Greenhalgh, Christian Jäger, Joanna Baginska, Paul Wilmes, Ro-
796 nan M.T. Fleming, and Ines Thiele. Generation of genome-scale metabolic reconstructions
797 for 773 members of the human gut microbiota. *Nature Biotechnology*, 35(1):81–89, 2017.

798 [44] Stefanía Magnúsdóttir and Ines Thiele. Modeling metabolism of the human gut micro-
799 biome. *Current Opinion in Biotechnology*, 51:90–96, 2018.

[45] R. A. Majewski and M. M. Domach. Simple constrained-optimization view of acetate overflow in E. coli. *Biotechnology and Bioengineering*, 35(7):732–738, 1990.

[46] Paola Mastromarino, Daniela Capobianco, Giuseppe Campagna, Nicola Laforgia, Pietro Drimaco, Alessandra Dileone, and Maria E. Baldassarre. Correlation between lactoferrin and beneficial microbiota in breast milk and infant's feces. *BioMetals*, 27(5):1077–1086, 2014.

[47] Susan Mills, Fergus Shanahan, Catherine Stanton, Colin Hill, Aidan Coffey, and R. Paul Ross. Movers and shakers Influence of bacteriophages in shaping the mammalian gut microbiota. *Gut Microbes*, 4(1):4–16, jan 2013.

[48] Amir Mitchell, Gal H. Romano, Bella Groisman, Avihu Yona, Erez Dekel, Martin Kupiec, Orna Dahan, and Yitzhak Pilpel. Adaptive prediction of environmental changes by microorganisms. *Nature*, 460(7252):220–224, 2009.

[49] G. Moro, S. Arslanoglu, B. Stahl, J. Jelinek, U. Wahn, and G. Boehm. A mixture of prebiotic oligosaccharides reduces the incidence of atopic dermatitis during the first six months of age. *Archives of Disease in Childhood*, 91(10):814–819, 2006.

[50] Elad Noor, Hulda S. Haraldsdóttir, Ron Milo, and Ronan M.T. Fleming. Consistent Estimation of Gibbs Energy Using Component Contributions. *PLoS Computational Biology*, 9(7), 2013.

[51] L. Nylund, M. Nermes, E. Isolauri, S. Salminen, W. M. De Vos, and R. Satokari. Severity of atopic disease inversely correlates with intestinal microbiota diversity and butyrate-producing bacteria. *Allergy: European Journal of Allergy and Clinical Immunology*, 70(2):241–244, 2015.

[52] Jeffrey D. Orth, Ines Thiele, and Bernhard O. Palsson. What is flux balance analysis? *Nature Biotechnology*, 28(3):245–248, 2010.

[53] Chana Palmer, Elisabeth M. Bik, Daniel B. DiGiulio, David A. Relman, and Patrick O. Brown. Development of the human infant intestinal microbiota. *PLoS Biology*, 5(7):1556–1573, 2007.

[54] Stephan Parche, Doris Jacobs, Fabrizio Arigoni, Fritz Titgemeyer, and Ivana Jankovic. Lactose-over-Glucose Preference in Bifidobacterium longum NCC2705: glcP, Encoding a

Glucose Transporter, Is Subject to Lactose Repression†. *Society*, 188(4):1260–1265, 2006.

[55] Van T. Pham, Christophe Lacroix, Christian P. Braegger, and Christophe Chassard. Early colonization of functional groups of microbes in the infant gut. *Environmental microbiology*, 18(7):2246–2258, 2016.

[56] Van Thanh Pham, Christophe Chassard, Etienne Rifa, Christian Braegger, Annelies Geirnaert, Vanesa Natalin Rocha Martin, and Christophe Lacroix. Lactate Metabolism Is Strongly Modulated by Fecal Inoculum, pH, and Retention Time in PolyFermS Continuous Colonic Fermentation Models Mimicking Young Infant Proximal Colon. *mSystems*, 4(4), 2019.

[57] Michael Jakob Pichler, Chihaya Yamada, Bashar Shuoker, Camila Alvarez-Silva, Aina Gotoh, Maria Louise Leth, Erwin Schoof, Toshihiko Katoh, Mikiyasu Sakanaka, Takane Katayama, Chunsheng Jin, Niclas G. Karlsson, Manimozhiyan Arumugam, Shinya Fushinobu, and Maher Abou Hachem. Butyrate producing colonic Clostridiales metabolise human milk oligosaccharides and cross feed on mucin via conserved pathways. *Nature Communications*, 11(1), 2020.

[58] Svenja Plöger, Friederike Stumpff, Gregory B. Penner, Jörg Dieter Schulzke, Gotthold Gäbel, Holger Martens, Zanming Shen, Dorothee Günzel, and Joerg R. Aschenbach. Microbial butyrate and its role for barrier function in the gastrointestinal tract. *Annals of the New York Academy of Sciences*, 1258(1):52–59, 2012.

[59] Chitong Rao, Katharine Z. Coyte, Wayne Bainter, Raif S. Geha, Camilia R. Martin, and Seth Rakoff-Nahoum. Multi-kingdom ecological drivers of microbiota assembly in preterm infants. *Nature*, 591(7851):633–638, 2021.

[60] M. Rogosa. the Genus Veillonella. I. General Cultural, Ecological, and Biochemical Considerations. *Journal of Bacteriology*, 87:162–170, 1964.

[61] F. F. Rubaltelli and G. Largajolli. Effect of Light Exposure on Gut Transit Time in Jaundiced Newborns. *Acta Pædiatrica*, 62(2):146–148, 1973.

[62] Christian F.P. Scholz and Mogens Kilian. The natural history of cutaneous propionibacteria, and reclassification of selected species within the genus propionibacterium to the proposed novel genera acidipropionibacterium gen. Nov., cutibacterium gen. nov. and

pseudopropionibacterium gen. nov. *International Journal of Systematic and Evolutionary Microbiology*, 66(11):4422–4432, 2016.

[63] Robert Schuetz, Lars Kuepfer, and Uwe Sauer. Systematic evaluation of objective functions for predicting intracellular fluxes in Escherichia coli. *Molecular Systems Biology*, 3(119), 2007.

[64] Clarissa Schwab, Hans Joachim Ruscheweyh, Vera Bunesova, Van Thanh Pham, Niko Beerenwinkel, and Christophe Lacroix. Trophic interactions of infant bifidobacteria and eubacterium hallii during L-fucose and fucosyllactose degradation. *Frontiers in Microbiology*, 8:1–14, 2017.

[65] Sudarshan A. Shetty, Simone Zuffa, Thi Phuong Nam Bui, Steven Aalvink, Hauke Smidt, and Willem M. De Vos. Reclassification of eubacterium hallii as Anaerobutyricum hallii gen. nov., comb. nov., and description of Anaerobutyricum soehngenii sp. nov., a butyrate and propionate-producing bacterium from infant faeces. *International Journal of Systematic and Evolutionary Microbiology*, 68(12):3741–3746, 2018.

[66] Yuli Song, Chengxu Liu, and Sydney M Finegold. Bacteroides. In *Bergey's Manual of Systematics of Archaea and Bacteria*, pages 1–24. Wiley, sep 2015.

[67] Norbert Sprenger, Hannah Odenwald, Anna Kaarina Kukkonen, Mikael Kuitunen, Erkki Savilahti, and Clemens Kunz. FUT2-dependent breast milk oligosaccharides and allergy at 2 and 5 years of age in infants with high hereditary allergy risk. *European Journal of Nutrition*, 56(3):1293–1301, 2017.

[68] P. L. Stark and A. Lee. The microbial ecology of the large bowel of breast-fed and formula-fed infants during the first year of life. *Journal of Medical Microbiology*, 15(2):189–203, 1982.

[69] Naoki Tsukuda, Kana Yahagi, Taeko Hara, Yohei Watanabe, Hoshitaka Matsumoto, Hiroshi Mori, Koichi Higashi, Hirokazu Tsuji, Satoshi Matsumoto, Ken Kurokawa, and Takahiro Matsuki. Key bacterial taxa and metabolic pathways affecting gut short-chain fatty acid profiles in early life. *ISME Journal*, 2021.

[70] Francesca Turroni, Christian Milani, Sabrina Duranti, Gabriele Andrea Lugli, Sergio Bernasconi, Abelardo Margolles, Francesco Di Pierro, Douwe Van Sinderen, and Marco

887 Ventura. The infant gut microbiome as a microbial organ influencing host well-being.
888 *Italian Journal of Pediatrics*, 46(1):1–13, 2020.

889 [71] Carla C. Uranga, Pablo Arroyo, Brendan M. Duggan, William H. Gerwick, and Anna
890 Edlund. Commensal Oral Rothia mucilaginosa Produces Enterobactin, a Metal-Chelating
891 Siderophore. *mSystems*, 5(2), 2020.

892 [72] J. Valentin and Christian Streffer. Basic anatomical and physiological data for use in
893 radiological protection: Reference values - ICRP Publication 89. *Annals of the ICRP*,
894 32(3-4):1–277, 2002.

895 [73] P. Van den Abbeele, C. Duysburgh, E. Vazquez, J. Chow, R. Buck, and M. Marzorati.
896 2 -Fucosyllactose alters the composition and activity of gut microbiota from formula-fed
897 infants receiving complementary feeding in a validated intestinal model. *Journal of Func-*
898 *tional Foods*, 61(July):103484, 2019.

899 [74] Milan J.A. van Hoek and Roeland M.H. Merks. Redox balance is key to explaining full vs.
900 partial switching to low-yield metabolism. *BMC Systems Biology*, 6, 2012.

901 [75] Milan J.A. van Hoek and Roeland M.H. Merks. Emergence of microbial diversity due to
902 cross-feeding interactions in a spatial model of gut microbial metabolism. *BMC Systems*
903 *Biology*, 11(1):1–18, 2017.

904 [76] Katrien M.J. Van Laere, Tjakko Abee, Henk A. Schols, Gerrit Beldman, and Alphons G.J.
905 Voragen. Characterization of a novel β-galactosidase from Bifidobacterium adolescentis
906 DSM 20083 active towards transgalactooligosaccharides. *Applied and Environmental Mi-*
907 *crobiology*, 66(4):1379–1384, 2000.

908 [77] Sander S. Van Leeuwen, Bas J.H. Kuipers, Lubbert Dijkhuizen, and Johannis P. Kamerling.
909 1 H NMR analysis of the lactose/β-galactosidase-derived galacto-oligosaccharide compo-
910 nents of Vivinal® GOS up to DP5. *Carbohydrate Research*, 400:59–73, 2014.

911 [78] David M. Versluis, Ruud Schoemaker, Ellen Looijesteijn, Daniël Muysken, Prescilla V.
912 Jeurink, Marcel Paques, Jan M. W. Geurts, and Roeland M. H. Merks. A Multiscale Spa-
913 tiotemporal Model Including a Switch from Aerobic to Anaerobic Metabolism Reproduces
914 Succession in the Early Infant Gut Microbiota. *mSystems*, 2022.

[79] Thomas Wolever Vogt and Janet. Human Nutrition and Metabolism to Acetate Absorption from the. *American Society for Nutritional Sciences*, 133(10):3145–3148, 2003.

[80] Paul Vos, George Garrity, Dorothy Jones, Noel R Krieg, Wolfgang Ludwig, Fred A Rainey, Karl-Heinz Schleifer, and William B Whitman. *Bergey's manual of systematic bacteriology: Volume 3: The Firmicutes*, volume 3. Springer Science & Business Media, 2011.

[81] Harm Wopereis, Kathleen Sim, Alexander Shaw, John O. Warner, Jan Knol, and J. Simon Kroll. Intestinal microbiota in infants at high risk for allergy: Effects of prebiotics and role in eczema development. *Journal of Allergy and Clinical Immunology*, 141(4):1334–1342.e5, 2018.

[82] Xinqiang Wu, Yuanbing Wu, Liangmei He, Longhuo Wu, Xiangcai Wang, and Zhiping Liu. Effects of the intestinal microbial metabolite butyrate on the development of colorectal cancer. *Journal of Cancer*, 9(14):2510–2517, 2018.

[83] Shin Ichiro Yokoyama and Tohru Suzuki. Isolation and characterization of a novel equol-producing bacterium from human feces. *Bioscience, Biotechnology and Biochemistry*, 72(10):2660–2666, 2008.

[84] Bryan Zabel, Christian Clement Yde, Paige Roos, Jørn Marcussen, Henrik Max Jensen, Krista Salli, Johanna Hirvonen, Arthur C. Ouwehand, and Wesley Morovic. Novel Genes and Metabolite Trends in Bifidobacterium longum subsp. infantis Bi-26 Metabolism of Human Milk Oligosaccharide 2'-fucosyllactose. *Scientific Reports*, 9(1):1–11, 2019.